THE
PHYSICAL REVIEW
A journal of experimental and theoretical physics established by E. L. Nichols in 1893

SECOND SERIES, VOL. 64, NOS. 1 AND 2 JULY 1 AND 15, 1943

The Spatial Asymmetry of Cerenkov Radiation as a Function of Electron Energy*

HAROLD O. WYCKOFF** AND J. E. HENDERSON
University of Washington, Seattle, Washington
(Received April 1, 1943)

The properties of the radiation discovered in 1934 by P. A. Cerenkov when high speed electrons traverse transparent media has been studied as a function of the energy of the bombarding particle. It is found that the direction of emission of the radiation for mica over the range from 240 to 815 kv is given by the relation proposed by Frank and Tamm, where $\cos\theta = 1/\beta n$, θ being the angle of progression of the radiation with the electron beam and n, the index of refraction of the mica used as the target. In this range β changes markedly, providing a significant test of this relation as a function of the energy of the bombarding particle. The experiments were carried out with the use of a transformer-rectifier source of potential and an electron tube giving a well-collimated beam of electrons.

INTRODUCTION

THE emission of a visible radiation with remarkable asymmetry properties when high speed electrons bombarded transparent materials was first discovered and investigated by Cerenkov[1] in 1934. This radiation, continuous in character, and appearing as a bluish white light proceeds from the point of impact of the electrons at an angle of the order of 30° with the direction of the electron beam. The nature of this radiation was formulated by Frank and Tamm[2] who recognized that the electrons causing this radiation are travelling through the media with a velocity greater than the velocity of light which they produce. A simple Huygens construction showing the formation of such a wave front when a high energy electron enters a transparent material is illustrated in Fig. 1. A cone of visible radiation appears in the medium with apex at the point of entrance of the elec-

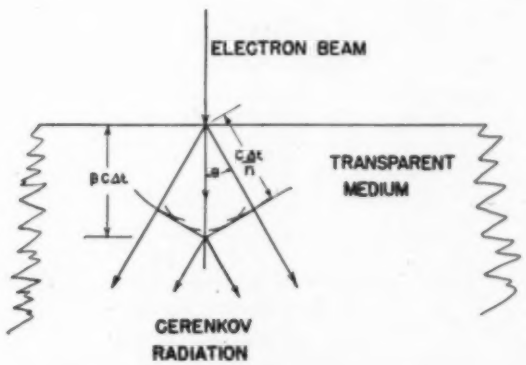

FIG. 1. Simple Huygens construction illustrating the formation of the wave fronts in the production of Cerenkov radiation. The electrons producing the radiation travel faster in the transparent medium than does the radiation which they generate. The radiation is symmetrical about the electron beam.

* Presented at the Seattle Meeting of the American Physical Society, June 18–21, 1940.

** Now at the National Bureau of Standards, Washington, D. C.

[1] P. A. Cerenkov, Comptes rendus Acad. Sci., U.S.S.R. **2**, 451 (1934); **3**, 414 (1936); **14**, 101 (1937); **14**, 105 (1937). Phys. Rev. **52**, 378 (1937).

[2] I. Frank and Ig. Tamm, Comptes rendus Acad. Sci., U.S.S.R. **14**, 109 (1937).

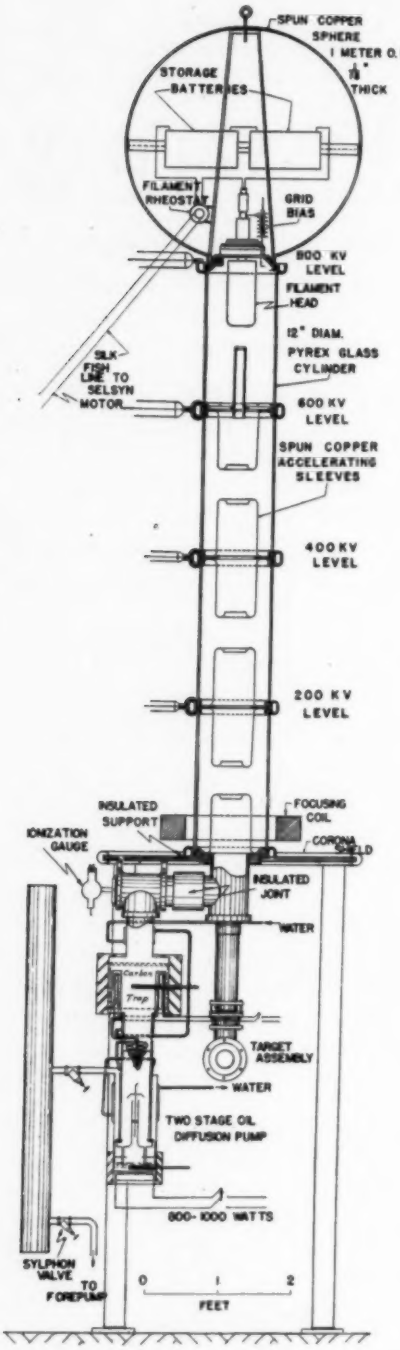

FIG. 2. A schematic diagram of the tube in which the high energy electrons are generated.

trons. From this construction it is evident that:

$$\cos\theta = 1/\beta n, \qquad (1)$$

where β is the ratio of the velocity of the electron in the medium to the velocity of light in a vacuum and n is the index of refraction of the medium for the visible light observed.

A classical calculation of the energy to be expected in such a process has also been given by Frank and Tamm and later by Fermi.[3] A quantitative experimental investigation of this radiation has been made by Collins and Reiling[4] who have demonstrated that Eq. (1) holds within their experimental limits for mica, Cellophane, and glass targets as far as the dependence of the angle of emission upon the index of refraction is concerned. Their work can scarcely be regarded as a complete verification of this equation as one value of β only was used, namely, that corresponding to 1.9 Mev. In this region β changes very little with the energy of the impinging electron. The present experiment was designed primarily to investigate the dependence of the angle of emission upon the energy of the impinging electron in a region where β changes sufficiently to provide a further test of Eq. (1) as far as the dependence of θ upon β is concerned. Specifically this involved the measurement of the angle of emission of the radiation caused by a well-collimated beam of high energy electrons impinging on a thin target of mica.

APPARATUS AND PROCEDURE

A schematic diagram of the tube in which the high energy electrons were generated and the auxiliary apparatus is shown in Fig. 2. The tube, which was designed for operation at potentials up to 800 kv, consists of four sections to which the voltage was applied in successive steps of up to 200 kv each. The circuit design and voltage wave form of this particular Villard-type supply may be found elsewhere.[5] This supply is part of the super-voltage x-ray equipment installed by the General Electric X-Ray Corporation at the Swedish Hospital in Seattle. The bronze castings holding the accelerating sleeves were separated with Pyrex cylinders 1 foot in diameter and 2 feet long. At the top of the tube a one-meter sphere of spun copper serves as a corona shield for the filament and grid supply. The target assembly, pumping

[3] E. Fermi, Phys. Rev. **57**, 485 (1940).
[4] G. B. Collins and V. G. Reiling, Phys. Rev. **54**, 499 (1938).
[5] J. E. Henderson, J. E. Rose, and W. H. Goss, Rev. Sci. Inst. **6**, 63 (1935).

system, and magnetic focusing coil are located at the base of the tube.

The pumping system consisted of a carbon trap used in conjunction with a two-stage oil diffusion pump[6] having a speed of approximately 100 liters per second. The carbon trap was used primarily to eliminate oil vapors from the tube to obtain a maximum filament life in both the gauges and cathode. Although not necessary for operation of the pump, a fore-vacuum of less than two microns was maintained as measured by an oil McLeod gauge. This permitted a tube vacuum of better than 2×10^{-6} mm Hg which rose to about twice this value during operation. The entire pumping system is insulated from the tube proper by a mica and wax joint to facilitate the measurement of tube currents.

The cathode head is shown in Fig. 3. It faces a small acceleration electrode which may be screwed in or out of the casting at 600 kv for adjusting the distance between the electrodes in the top section. Since each accelerating sleeve is really an electrostatic lens this distance of separation is important and particularly so in the first section. The filament and focusing cup are insulated from each other and from the filament housing. As the voltage supply is pulsating d.c., this makes possible the placing of a negative potential on the cup so that appreciable current passes through the tube only near the peak of the cycle. These parts may also be individually adjusted vertically by means of the sylphons and adjusting nuts without breaking the vacuum. A double eccentric similar to that used by Tuve[7] and Taylor[8] permits the lateral adjustment of the whole filament with an amplitude of about 1 cm in every direction from the axis of the tube. An insulating band midway along the top section supports a permanent magnet whose distance from the axis of the tube is adjustable. Adjustment of these variables aids materially in the final focusing of the tube.

The Cerenkov radiation under investigation in this experiment was also used as an aid in focusing the tube. A sheet of mica was mounted at the bottom of the top accelerating sleeve in the section at 600 kv and the normal potential was applied across the top section of the tube. By adjustment of the focusing variables the electron beam was brought to the tube axis and its size adjusted. This focused condition was shown by the appearance of a bright spot of Cerenkov radiation on the axis at the tube at the point of impact of the electrons on the mica. The same procedure was repeated for each section of the tube. During the initial focusing of the tube it was found necessary to install a short length of 8″ diameter Pyrex tubing in the section between the 600- and 400-kv levels coaxial with the 12″ diameter tubing to eliminate puncture of the main Pyrex cylinders. The beam as it emerges from the bottom of the tube is diverging. The magnetic focusing coil at the bottom of the tube permitted compensation so that the beam was sensibly parallel. The current required for this depended upon the energy of

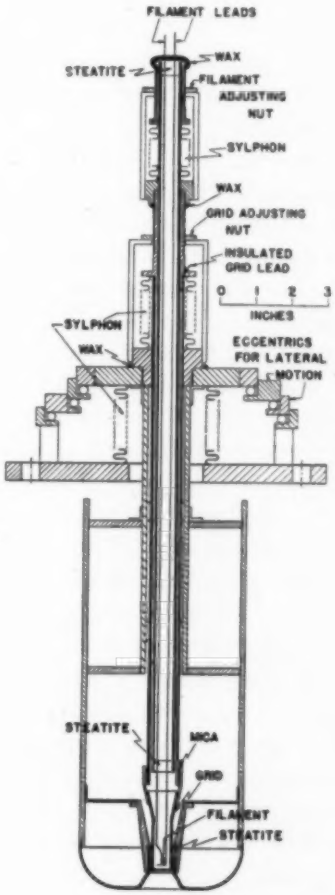

FIG. 3. The cathode assembly. The double eccentric permits a lateral adjustment of the whole cathode.

[6] J. E. Henderson, Phys. Rev. **50**, 388 (1936).
[7] M. A. Tuve, Phys. Rev. **48**, 241 (1935).
[8] L. S. Taylor, J. Research Nat. Bur. Stand. **21**, 19 (1938).

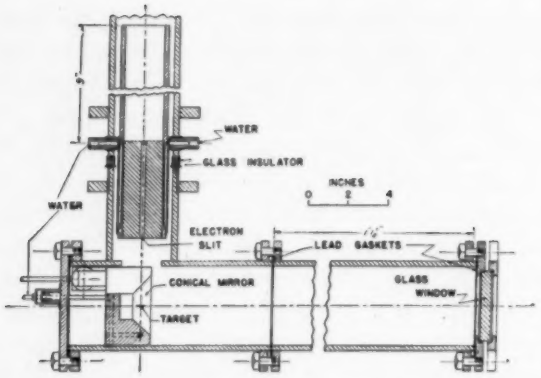

FIG. 4. The target and electron slit assembly. The electrons strike the mica target located on the axis of a 45° conical mirror. Radiation proceeding in a plane perpendicular to this axis is reflected parallel to the axis.

the electrons and provided a means of selecting electrons of a particular energy for the experiment.

The target and electron slit assembly are shown in Fig. 4. A water-cooled double slit of $\frac{1}{16}''$ diameter defines the electron beam at the bottom of the tube so that it has a maximum divergence of about $\frac{3}{4}°$. This collimated beam falls on a mica target in which it produces the Cerenkov radiation. The surface of the mica intersects the axis of an insulated and water-cooled conical mirror of silver with a $\frac{1}{2}$ angle of 45° so that all radiation produced in the mica which is traveling in a plane perpendicular to the axis of the cone is reflected by the mirror into rays parallel to this axis. By this arrangement rays emerging from the mica in that plane will, after reflection from the mirror, appear along the arc of a circle. The position along this circle gives the angle of the ray with the electron beam. These rays then pass from the vacuum through a thick glass plate at the end of the tube housing the mirror. It was necessary to place this window at considerable distance from the target to avoid discoloration from x-rays and electrons necessarily present there. From here the rays passed through a hole in a $2\frac{1}{2}$-foot concrete wall to a lens system and camera where they were focused on a strip of photographic film. The wall was necessary for the protection of both the film and observers from the extremely penetrating x-rays which were also produced by the tube. In order to obtain the radiation through the surface of the target without total internal reflection the surface of the mica is tilted at an angle with the electron beam. The mica was mounted so that it could be tilted at an angle of 20° in either direction by the mechanism shown in Fig. 5, where the target is fastened to an axle through the axis of the cone which may be rotated by air pressure through a total of 40°. Radiation should therefore appear at equal angles with the beam when the axle is rotated to its two extreme positions. The target was adjusted until these readings were equal within the accuracy of measurement. The mica used as targets in the final experiments was 0.001 inch and 0.00005 inch thick and came from two independent sources. With these thicknesses the average energy loss in the mica is small and sharp images were obtained. With extremely thin layers of mica the intensity of the radiation is small. The thicknesses chosen were really a compromise between these two factors.

The current to the target was indicated by the deflection of an oscilloscope which was placed across a high resistance in series with the lead from the target to ground. A background which existed on the screen of the oscillograph due to the current induced in the target-ground leads by the potential on the tube gave a means of determining the phase of the target current. An electronic switch which was used in the initial experiments was found unnecessary because of this effect.

The final focusing of the tube was attained for the different voltages by means of the large electromagnetic focusing coil around the lowest section of the tube. The current to this coil was adjusted so that the target current peak appeared superimposed on the peak of the voltage wave. In general this current peak was not more than 20 electrical degrees in width. A current of 10^{-6} ampere was sufficient to give intensities

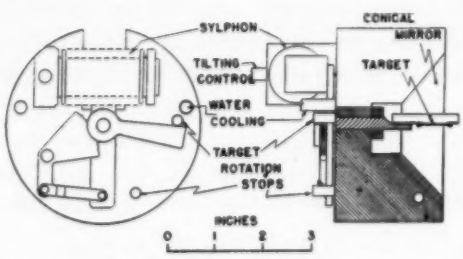

FIG. 5. Target tilting mechanism. The target must be tilted to avoid total reflection at the surface.

strong enough for recording. The voltage indicated by a sphere gap which was previously calibrated against a rotary voltmeter[5] was therefore a measure of the energy of the electrons producing the radiation.

RESULTS

A series of pictures of the radiation was taken over the voltage range from 240 to 815 kv. Typical pictures are shown in Fig. 6. The bright spot at the bottom is the image of the filament. One exposure was made with a variable voltage and with both positions of the mica so that the two spots were spread into a large arc on each side of the filament image. An enlarger was used to focus the image of this negative on the periphery of a small protractor. The angles of all of the other exposures were then measured by the protractor for the same setting of the enlarger. Actually, due to the finite width of slits and range of energies possible, the image is not a point but a narrow band. The mean of the upper and lower limits of angle in the exposed arc measured from the filament image appearing at the lower edge of the mirror was taken as the true angle. This averaging was justified by calculations which showed, at least for short exposures, that the angular width of the radiation could be attributed to the finite resolving power of the electron slit. Longer exposures showed wider spreads in this angular width which was probably due to scattering of electrons in the thin mica target and could therefore be assumed to produce equal effects on each side of the mean.

800 kv 258 kv

FIG. 6. Typical pictures of the radiation with the mica tilted 20° to the electron beam. After reflection from the conical mirror the radiation appears along the arc of a circle. The angle measured along the arc from the filament image at the bottom gives the angle of emergence of the radiation from the mica. The shift in angle of emission of the radiation with energy of the electron beam is readily visible.

In all cases the total angular spread was so small that the rays at the average angle inside the mica were also at the average angle outside the mica after refraction within the error of measurement of angles.

The solid curve of Fig. 7, where the angle of the radiation in the mica is plotted against the energy of the electron producing it, shows the theoretical curve for the two samples of mica used. These values were calculated from Eq. (1)

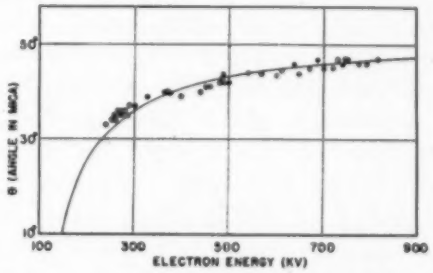

FIG. 7. The angle of progression of the radiation in mica as a function of the electron energy. The solid curve is the theoretical one obtained from Eq. (1). The open and closed circles represent experimental points obtained by two different samples of mica.

by substituting the index of refraction of 1.59 obtained for the mica film. The index of refraction of the mica was measured by the immersion method with the use of a petrographic microscope. Although mica is biaxial, two of its indices are so close together that for the experiment mica may be considered as uniaxial. The measured values of the index showed 1.59 as the proper value of the index to use in the computation. The experimental points are indicated by the small circles on these graphs. They are determined from the experimentally measured angles by taking into account the refraction of the radiation on emergence from the mica. The solid and open circles represent two different samples of mica with the same index of refraction. These experimental points for both samples all fall on the theoretical curve within our estimate of the limit of the experimental error. The functional dependence of the angle of emission of the radiation upon the velocity of the electron is that given by Eq. (1) within the range used in this experiment.

Although the deviation of the points at lower voltages from the theoretical curve is very close to our estimate of the limit of error of the

experiment, all the points, even after repeated check experiments, fall above the theoretical curve suggesting that in this region a possible deviation from theory may occur. Lower energy points are very difficult to obtain with this apparatus because of the focusing difficulties with such a long electron path. Experiments are in progress to facilitate more measurements in this region with a shorter tube to see if this suggested diversion is real or apparent.

The result of this research coupled with the experiment of Collins and Reiling provides strong evidence for the soundness of the theory of Frank and Tamm. Not only is there the proper dependence of the direction of emission upon the index of refraction but also the proper dependence upon the energy over the range from 240 kv to 815 kv in which region the angle of emission changes rapidly. To this should be added the single point obtained by Collins and Reiling at 1900 kv.

Since the agreement between theory and experiment must be regarded as satisfactory it is of interest to recall the basis upon which this theory is founded. The theory is entirely classical. This satisfactory application of classical continuum theory to the problem is not surprising as the problem is essentially one of propagation of radiation in a dielectric. For the radiation to be propagated as a wave front, destructive interference must occur in all directions except that in which propagation occurs. Evidently the substance bombarded must radiate coherently over at least one wave-length of the light observed. The displacement of the dispersion centers by the electron is evidently the same all along the path of the electron. The field surrounding the moving electron acts to polarize the medium resulting in a displacement of the dispersing centers supporting the proposal of Fermi that in the energy loss of high speed electrified particles passing through matter the polarization of the medium must be taken into account.

If the explanation is valid, an experiment of this type provides a means of determining the velocity of high speed electrified particles in terms of time and distance since the angle of emission depends upon the distance the particle moves in the time for the radiation to travel one wave-length of the light observed. The values of β used in computation of the theoretical curves are based upon the relativistic expression for the energy of a particle. In this same sense this expression is substantiated.

It is with pleasure that we acknowledge our debt to the Board of Directors and the Tumor Institute of the Swedish Hospital of Seattle and particularly to Dr. N. A. Johansen, Chairman of the Board, for placing their equipment at our disposal. We are also indebted to the Seattle City Light and the Puget Sound Light and Power Company for generous donation of materials and to the Service Shop of the General Electric Company for the use of their atomic hydrogen welding equipment.

Electrons in Equilibrium with the Penetrating Component of Cosmic Rays in Lead at 10,000 Feet and at Sea Level

WAYNE E. HAZEN
University of California, Berkeley, California

(Received April 8, 1943)

The number of electrons (N) in equilibrium with the penetrating component of the cosmic rays in lead at 10,000 ft. and at sea level has been measured with Wilson cloud chambers containing lead plates. The value for N obtained at 10,000 ft. is 7.4 ± 0.2 percent, at sea level 6.8 ± 0.6 percent. Comparison is made with values for N calculated from the equations of Bhabha and Tamm and Belenky with a mesotron mass of 200 m and Blackett's cosmic-ray spectrum. If the loss of low energy electrons as a result of scattering in the lead is taken into account, the calculated values for N are only slightly larger than the experimental values. If the calculated values for N are assumed to be correct, the present results provide additional evidence that protons constitute only a small fraction of the cosmic-ray particles in the lower atmosphere.

THE study of the production of high energy collision electrons by the penetrating component of cosmic rays provides information concerning the origin of the soft component since these collision electrons and their cascade progeny constitute an appreciable fraction of the soft component. The actual production of the collision electrons in air cannot be conveniently studied, hence it is customary to introduce denser materials in order to produce collision electrons more copiously in the relatively small region under observation. In the present type of experiment the greater ambiguity of measurements with G-M counter arrangements more than offsets the greater time required in obtaining results with the Wilson cloud-chamber technique. There have been several cloud-chamber determinations of the number of electrons (N) in equilibrium with the penetrating component in dense materials at sea level.[1–5] Practically all of these electrons are high energy collision electrons or their cascade progeny. The present report is concerned with the results of a cloud-chamber study of N at Tioga Pass, Yosemite National Park, California (9950 ft.), in 1942, together with the results of a redetermination of N at sea level from photographs taken by M. A. Starr[6] at Berkeley in 1937.

[1] B. Trumpy, Zeits. f. Physik **111**, 338 (1938).
[2] J. G. Wilson, Nature **142**, 73 (1938).
[3] J. I. Hopkins, W. M. Nielsen, and L. W. Nordheim, Phys. Rev. **55**, 233 (1939).
[4] W. M. Powell, Phys. Rev. **57**, 1061 (1940).
[5] L. Seren, Phys. Rev. **62**, 204 (1942).
[6] M. A. Starr, Phys. Rev. **53**, 6 (1938).

APPARATUS

The front portion of the cloud chamber was a 30×30 cm cylinder containing eight evenly-spaced horizontal lead plates. Each plate had a thickness of 0.6 cm which, together with the steel reflecting sheets glued to each face, constituted the equivalent of a thickness of 0.7 cm of lead. Illumination was provided by discharging a 150-μf condenser bank through each of two cylindrical (2×15 cm) Edgerton-type argon flash tubes. The condenser units were charged to 1800 v with a 2000-v d.c. motor-generator set. The light beams were directed forward and across the chamber at an angle of 50° with the chamber axis. The photographs were taken on Agfa Ultraspeed 35-mm film in a stereoscopic camera equipped with Leitz Hektor 135-mm lenses. With the camera at a distance of 180 cm from the chamber and lens stops of $f:9$ most of the pictures were overexposed. Expansions were made at the rate of one per minute without counter control. The clearing field was reduced one-half second before the expansion in order to lengthen the sensitive time for diffuse tracks; the sensitive time for sharp tracks was of necessity very short even at the optimum expansion ratio,[7] since the lead plates effectively divided the large chamber into a group of small chambers.

The photographs were observed stereoscopically with 5-cm lenses as simple magnifiers; where necessary more accurate observations could be made by reprojection through the camera itself

[7] W. E. Hazen, Rev. Sci. Inst. **13**, 247 (1942).

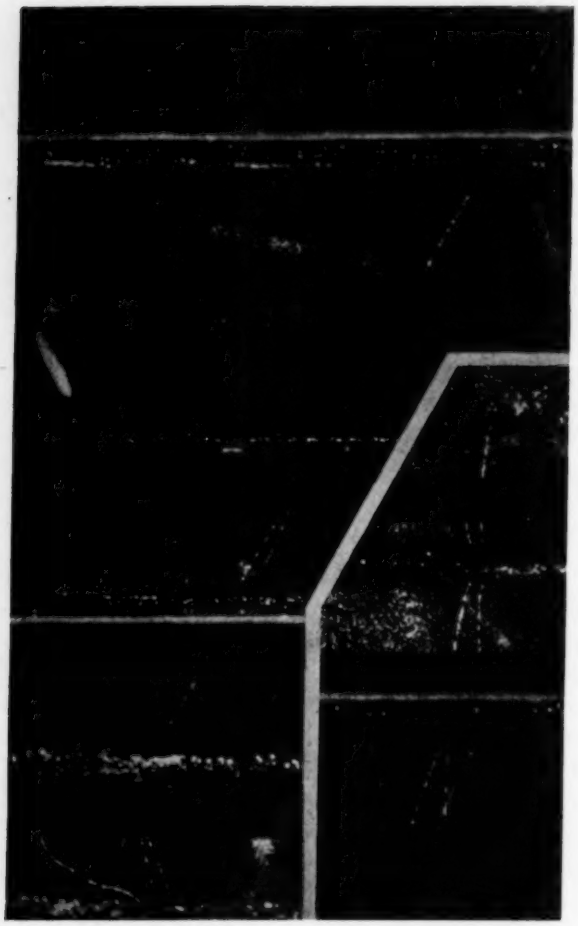

FIG. 1. Example of a penetrating ray accompanied by a single electron from one plate and a group of three electrons from another plate. The insert shows one of the few electrons that might possibly be confused with a mesotron. If the particle were a mesotron with sufficient energy to produce the accompanying electrons, it would continue through the lower plate.

onto an adjustable screen. Examples of the photographs are reproduced in Fig. 1.

RESULTS

Particles which passed through three or more of the lead plates without multiplying were listed as penetrating. From observations of the initial rate of multiplication of the high energy electrons observed in the same series of photographs, it is estimated that less than 0.1 percent of the particles listed as penetrating could have been electrons (see Fig. 1). About three-fourths of the traversals were classed as unsuitable for the observation of knock-on electrons and their progeny, either because they were not in the region of sharp focus or because of the presence of other tracks in the same region. Since only 2.7 percent of the collision electrons were sufficiently energetic to penetrate an additional lead plate, equilibrium was essentially established in the first plate (the correction would be negligible: an addition of one-eighth of 2.7 percent to the total number of accompanying electrons). In 13,260 traversals of a lead plate by a penetrating ray, 981 electrons were observed to emerge with the penetrating ray. Thus the probability (N) that an electron accompanies a penetrating ray in lead at 10,000 ft. is 7.4 ± 0.2 percent. There were five cases of three particles and three cases of four or more particles accompanying a penetrating ray; these were presumably mesotron-initiated electron showers. Two-particle cases were not considered separately from the general total since the probability of the chance occurrence of two unrelated accompanying electrons is of the same magnitude as the probability of occurrence of two shower electrons. Eight heavily ionizing particles were observed to accompany the penetrating rays in lead.

The probability of an electron accompanying a penetrating particle at sea level was redetermined by a study of the counter-controlled photographs taken by Starr.[6] A lead plate whose thickness varied from 0.65 to 1.65 cm in different sets of pictures was placed in the center of the cloud chamber, a 0.63-cm plate in the top of the cloud chamber, and a 0.37-cm plate above the top counter tube. Only those penetrating rays that passed through both of the plates in the cloud chamber were considered and electrons accompanying the selected penetrating rays from the lowest plate were counted. There were 148 electrons resulting from 2200 traversals, or a probability of 6.8 ± 0.6 percent that an electron accompanies a penetrating ray in lead at sea level.

DISCUSSION

The results of the present experiments are compared in Table I with those of previous investigations. In most cases the plate material was lead, in others it was gold or tungsten. The results can be compared directly, however, since the atomic numbers are nearly the same and the value of N varies less rapidly than the atomic

number. One of the reproduced photographs with its accompanying description in Trumpy's article[1] indicates that electrons were included whose relation to the penetrating component is questionable; this would explain his high value for N. Since Wilson's chamber was in a strong magnetic field,[2] many low energy electrons would not be observed; hence we expect a low value for the total number of electrons from his data. Seren's value of N for tungsten is rather high; however, the statistical uncertainty is larger than in the other determinations. The other values are in reasonable agreement but it appears likely that subjective errors are not negligible. The values of N determined by the same observer at sea level and at 10,000 ft. are not significantly different.

Bhabha[8] has given a theoretical expression for the number (N) of collision electrons and their cascade progeny accompanying a penetrating ray of given energy and mass. If we make the calculations for a mesotron mass of 200 m (the average of the reliable mass determinations), the results for electrons of all energies as a function of mesotron energy are those indicated in Table II. The average value ($\bar{N}$) for all mesotrons, obtained by a numerical integration of N over the Blackett[9] energy spectrum, is 11 percent. This result is considerably higher than the experimental result of 6.8 percent, but it is not far outside the uncertainty of 30 percent which Bhabha suggests for his equations.

A calculation of $\bar{N}$ was also made for the energy spectrum to be expected at 10,000 ft. The number of mesotrons in an energy band E to $E+dE$ at 10,000 ft. is the number in a band $E-(5\times10^8)$ to $E+dE-(5\times10^8)$ at sea level, since the energy lost in traversing 10,000 ft. of air is 5×10^8 ev. We must also consider the effect of mesotron decay in reducing the number of particles reaching sea level from 10,000 ft. If $n(10M)$ and $n(0)$ are the numbers of mesotrons at 10,000 ft. and sea level, respectively,

$$n(10M)/n(0)=\exp\left[\mu_0 c\Delta h/\tau_0 E\right],$$

where μ_0 and τ_0 are the mesotron mass and lifetime, respectively, Δh is the difference in elevations, and E is the effective energy (approximately the mean energy).[10] The best experimental value for $\mu_0 c/\tau_0$ is probably 1.2×10^3 ev/cm.[11] A numerical integration of N over a 10,000-ft. spectrum obtained as indicated above gives a value of ten percent for $\bar{N}$ whereas the value of $\bar{N}$ calculated for the sea-level spectrum is eleven percent. The difference in the calculated values for $\bar{N}$ at the two altitudes depends on the fact that the cross section for production of high energy collision electrons increases with mesotron energy but it does not depend critically on the details of the subsequent behavior of the collision electrons. Hence the uncertainty in the relative values of $\bar{N}$ is small compared with the uncertainty of 30 percent in the absolute magnitudes since the latter arises almost entirely from uncertainties in the calculations of the cascade process. The observed values for $\bar{N}$ at the two altitudes are not significantly different; as previously mentioned, there are probably other experimental errors at least as large as the statistical uncertainty.

Tamm and Belenky,[12] in a more detailed analysis of the problem, have derived an expression for the number of electrons $N(E)$ with energy greater than a given energy E in equilibrium with mesotrons. If we follow their

TABLE I. The number of electrons (N) in equilibrium with the penetrating component determined experimentally.

	Material	Number of traversals	N in percent	Statistical error
Trumpy (ref. 1)	Lead	800	17	±2
Wilson (ref. 2)	Gold	900	4.8	0.7
Hopkins *et al.* (ref. 3)	Lead	1600	11	1
Powell (ref. 4)	Lead	2500	8.2	0.6
Seren (ref. 5)	Tungsten	500	15	2
	Lead	600	9.7	1
Hazen Sea level	Lead	2200	6.8	0.6
Hazen 10,000 ft.	Lead	13000	7.4	0.2

TABLE II. The number of electrons (N) in equilibrium with a mesotron of mass 200 m and energy W calculated from Bhabha's equations.

W ev	4×10^8	10^9	10^{10}	10^{11}	10^{12}
N percent	0.6	5.4	18	26	32

[8] H. J. Bhabha, Proc. Roy. Soc. **A164**, 257 (1938).
[9] P. M. S. Blackett, Proc. Roy. Soc. **A159**, 1 (1937).
[10] B. Rossi and D. B. Hall, Phys. Rev. **59**, 223 (1941).
[11] B. Rossi, K. Greisen, J. C. Stearns, D. K. Froman, and P. G. Koontz, Phys. Rev. **61**, 675 (1942).
[12] Ig. Tamm and S. Belenky, J. Phys. Acad. Sci. U.S.S.R. **1**, 177 (1939).

method for obtaining numerical results, but use 200 m in place of 160 m for the mesotron mass and Blackett's energy spectrum in place of the Heisenberg-Euler spectrum, we obtain a value for $N(E)$ of fifteen percent with $E=10^6$ ev (twice the experimental result).

Scattering has been neglected. The effective lower limit for the energy of observed electrons is determined by the scattering in lead, since scattering decreases the component of an electron's range parallel to the mesotron path by a factor which increases with decreasing electron energy. Sheppard and Fowler[13] have found that the mean scattering angle (θ) for electrons with energy (E) less than 10^7 ev in thin lead plates of thickness (t) is approximately

$$\theta=500t^{\frac{1}{2}}/E,$$

where E is in Mev and θ in degrees. If we consider the mean scattering angle for an electron which has travelled one-tenth of its range, we find that

$$\theta=30E^{-\frac{1}{2}}.$$

Thus the observed number of one-Mev electrons would be greatly reduced by scattering, whereas the observed number of ten-Mev electrons would not be appreciably altered. An effective lower limit would be in the neighborhood of two or three Mev and the resulting value for $N(E)$ would be 7.5 or 8.5 percent, in substantial agreement with the experimental values.

E. J. Williams[14] has calculated values for $N(E)$ using cascade theory only in estimating the number of electrons with energy less than E. His results for $E=3\times10^6$ ev indicate a value for N between eight and thirteen percent in lead.

The agreement between experimental and theoretical values for the number of electrons in equilibrium with mesotrons in lead indicates that the theoretical values for air are probably about right. For air we obtain from the equations of Tamm and Belenky $N=11$ percent for $E=2.5\times10^6$ ev and $N=5.5$ percent for $E=10^7$ ev; Williams gives $N=12$ to 16 percent in air for $E=3\times10^6$ ev, and Rossi and Klapman[15] give $N=6.7$ percent for $E=10^7$ ev.

Considerable indirect evidence has already been accumulated indicating that high energy cosmic rays in the lower atmosphere are mostly mesotrons. The present results constitute another piece of evidence indicating that protons constitute only a minor fraction of the high energy cosmic rays if we assume that the theoretical values for N are correct. Since the number of electrons in equilibrium with protons of energy 10^{10} ev is only one-third as great as with mesotrons of the same energy and the number in equilibrium with protons of energy 3×10^9 ev is negligible, an admixture of ten or fifteen percent protons would lower N more than ten percent.

The author wishes to express his appreciation for the generous cooperation of Superintendent Frank A. Kittredge and other members of the staff of Yosemite National Park.

[13] C. W. Sheppard and W. A. Fowler, Phys. Rev. **57**, 273 (1940).

[14] E. J. Williams, Proc. Camb. Phil. Soc. **36**, 183 (1940).

[15] B. Rossi and S. J. Klapman, Phys. Rev. **61**, 414 (1942).

PHYSICAL REVIEW VOLUME 64, NUMBERS 1 AND 2 JULY 1 AND 15, 1943

The Photo-Conductivity of Lead Chromate

J. E. GOLDMAN* AND A. W. LAWSON
Randal Morgan Laboratory of Physics, University of Pennsylvania, Philadelphia, Pennsylvania
(Received December 9, 1942)

The variation of the photo-conductivity of lead chromate with wave-length of the exciting radiation is described. The conductivity referred to unit intensity of the incident radiation is a maximum in the blue corresponding to a value of 5×10^{-3} amp./watt at saturation. Subsidiary maxima occur in the red and the near ultraviolet. These results are in conflict with that of previous investigations. Data on the spectral scattering of lead chromate are also presented. The dependence of photo-conductivity on time, electric field, and previous history of the specimen are illustrated. On the basis of unit quantum efficiency, the mean displacement distance of photoelectrons in lead chromate is found to be 3×10^{-3} cm. Various alternative explanations of the observed behavior are discussed.

INTRODUCTION

MANY crystalline substances are affected by radiation lying in the visible or near ultraviolet portion of the spectrum. Thus, copper oxide, selenium, and properly prepared specimens of zinc sulphide become conducting when exposed to radiations of suitable wave-lengths, whereas the silver and thalium halides darken under similar exposure. Undoubtedly the most extensive experimental investigations of the sensitivity of solids to light are those conducted by Pohl[1] and his collaborators on the alkali halides containing a stoichiometric excess of alkali metal atoms, and those conducted by various investigators[2] on the blackening of silver bromide. The development of the theory of solids during the last decade has brought with it a fairly complete interpretation of the photosensitivity of these materials and suggests that similar interpretive work may be possible in many other cases that are of practical as well as scientific interest.

One of the most interesting cases of this type centers about the darkening of lead chromate, which forms the basis of the chrome yellow pigments. Depending upon the manner of preparation, this material exhibits varying degrees of darkening when exposed to ordinary sunlight. Since this substance appears to offer a number of interesting complexities not found in the materials studied hitherto, it was decided that it should be made the subject of extensive investigations designed to reveal the source of the light sensitivity.

The present paper deals with the light absorption and the photo-conductivity of lead chromate in the visible and very near ultraviolet region of the spectrum. Subsequent papers will deal with both thermal and optical darkening of the material and with the factors that influence its conductivity when not exposed to light. As will be seen in these subsequent papers, this work permits a reasonable and unambiguous interpretation of the mechanism of darkening by light.

METHOD

Difficulty in obtaining large single crystals of lead chromate necessitates the use of the powdered pigment. The commercial preparation is found to be a relatively poor photo-conductor. It is consequently necessary to study specially purified lead chromate. The samples are composed of fine needles about 0.45 micron in diameter. The preparation of satisfactory specimens is complicated by the fact that lead chromate is insoluble in all the usual solvents except metal hydroxides and cannot be melted without suffering marked structural changes. The obvious solution of this difficulty would seem to be, at first thought, to obtain specimens in the form of pressed pellets. This type of specimen, however, does not prove satisfactory because of the difficulty of preparing pressed pellets which are sufficiently dry. In such

*Now at Westinghouse Research Laboratories, East Pittsburgh, Pennsylvania.

[1] See the survey article by R. W. Pohl, Physik. Zeits. **39**, 36 (1938).

[2] A short résumé of this work appears in Chapter XVII of *Modern Theory of Solids* by F. Seitz (McGraw-Hill, New York, 1940); see also a survey article by J. H. Webb, J. App. Phys. **11**, 19 (1940); Mott and Gurney, *Electronic Processes in Ionic Crystals* (Oxford, London, 1940).

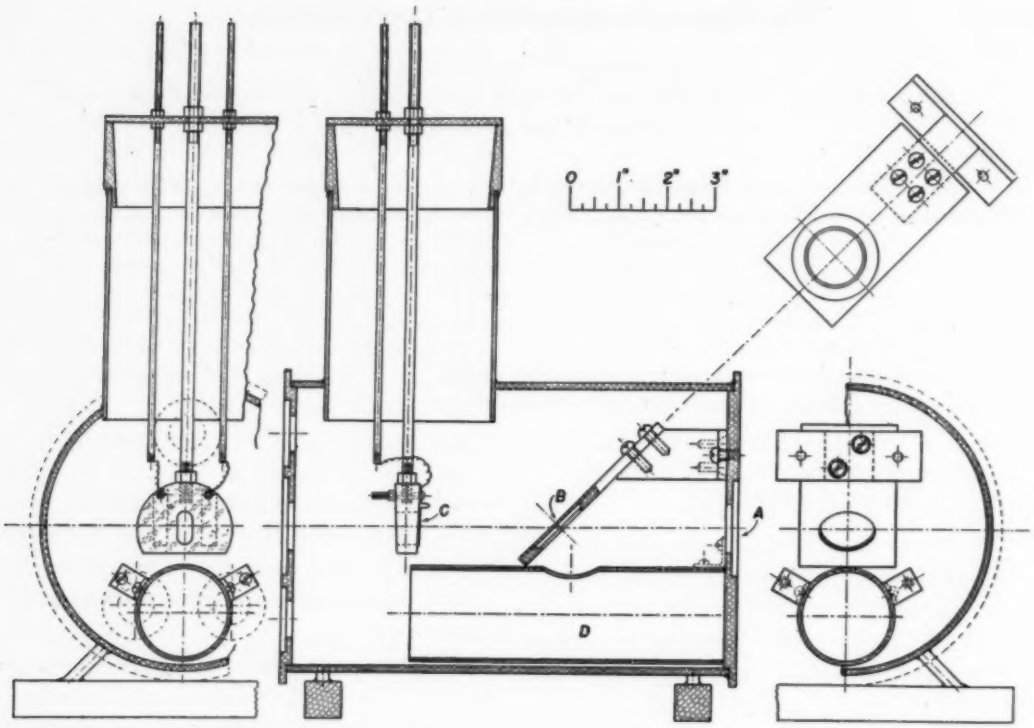

FIG. 1. Vacuum mount for specimen and photo-cell. In the center is shown a side view of the chamber. The beam of light enters through the quartz window *A*. Most of it is transmitted through the inclined quartz plate *B* and falls upon the specimen mounted on the leucite block *C*. The remaining light is reflected by the plate onto the photo-cell at *D*.

pellets, the dark currents arising from the moisture absorbed during pressing are sufficient to mask the smaller photo-currents. It is found necessary, therefore, to prepare specimens in such a way that the initially dried powder is not subsequently exposed to the slightest trace of water vapor. This is accomplished by drying the powder in a cell constructed from microscope slides. One slide contains a hole $\frac{3}{4}''$ in diameter and rests on top of another, thus forming a shallow disk-like container into which the loose powder is tamped. The cell and pigment are then baked in a furnace at 100°C for 24 hours. While the cell is still hot, a third slide is placed on the other two and the combined cell is sealed tightly with ceresin wax. The cover slide is of Corex D glass on which are evaporated suitable aluminum electrodes. The cell is supported against a leucite block by means of phosphor bronze clips which also serve to make electrical contact with the electrodes. The leucite block is then suspended in a vacuum chamber in such a manner that the specimen intercepts a beam of light admitted to the chamber by a quartz window. The aluminum electrodes are arranged to expose to the light a rectangular aperture 2 cm × 2 mm.

The light source consists of a water-cooled, high pressure mercury arc designated by the General Electric Company as type H-6. The luminous flux of the lamp is focused by a quartz lens onto a slit placed in front of a concave metal grating conjugate to the plane of the specimen. This grating has a one-meter focal length and the 15,000 lines per inch are ruled to give maximum intensity in the second order. The grating and specimen are on a standard Rowland mounting except that the position of the light source and the specimen are interchanged. This is done in order that the specimen may be illuminated by various wave-lengths with a minimum of electrical disturbance.

The photo-currents are measured by means of a three-stage d.c. amplifier described by Harnwell and Ridenour.[3] The first stage is an electrometer

[3] G. P. Harnwell and L. N. Ridenour, Rev. Sci. Inst. 11, 346 (1940).

tube mounted in an evacuated chamber to reduce the humidity about the input resistance. The vacuum chamber is made of steel $\frac{1}{2}''$ thick to serve as a magnetic and electric shield. The overall sensitivity is 2×10^{-17} amp./mm. A PJ-22 vacuum photo-cell and amplifier circuit is used to monitor the intensity of the incident light. The photo-cell is directly beneath a quartz plate inclined at 45 degrees to the incident beam as shown in Fig. 1. The incident light is split into two beams so that 95 percent is transmitted through the window and allowed to fall upon the specimen, and the remaining 5 percent is reflected down to the photo-cell. The amplified photo-cell current and the photo-currents in the specimen are determined simultaneously.

The spectral sensitivity of the photo-cell is determined by comparing the output of the cell with that of a thermopile calibrated in terms of a standard lamp. The calibration of the photo-cell is accomplished by placing the thermopile in the specimen mount in the place normally occupied by the specimen. Thus, the same fraction of light that falls on the specimen in an actual experiment is now incident on the thermopile. The output of the thermopile is determined by a low resistance galvanometer. An optical path of 8 meters is used with the galvanometer to assure an accuracy of 1 percent in the thermopile readings. This calibration is necessary since the spectral sensitivity of the photo-cell may deviate appreciably from the industrial calibration curve furnished by the manufacturer because of aging and temperature effects.

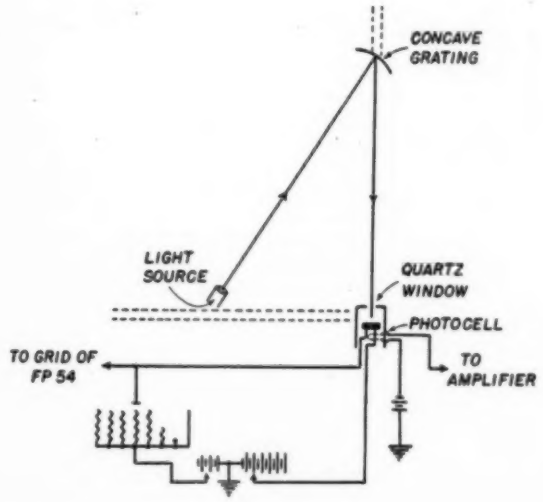

FIG. 2. Circuit diagram of the apparatus for the spectral photo-conductivity measurements.

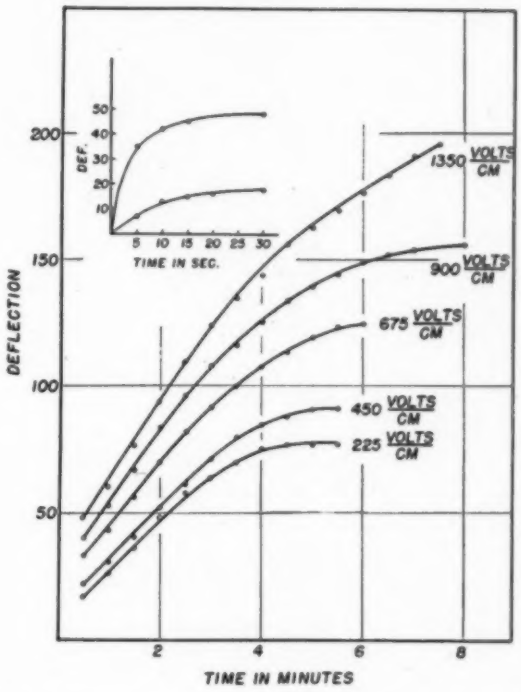

FIG. 3. Dependence of the photo-conductivity upon time in pure powdered lead chromate for various applied fields. The inset gives the first 30-second interval in greater detail for the lowest and highest voltage. 50 scale divisions correspond to a current of 1×10^{-7} amp.

Batteries supply any desired voltage up to 360 volts to the specimen. This corresponds to a field of 1350 volts/cm for the slit width used in these experiments. A potentiometer is used to balance out the dark currents which are of the same order of magnitude as the photo-currents. All batteries are contained in a drying box and shielded. A circuit diagram of the apparatus appears in Fig. 2.

RESULTS

Preliminary to an investigation of the spectral sensitivity of the photo-conductivity, it is necessary to examine the dependence of photo-conductivity on time of exposure and applied field. This is accomplished by impressing fields ranging from 225 to 1350 volts/cm upon the specimen and noting the resulting photo-conductivity for specified times of illumination. Figure 3 shows the results of this preliminary investigation. The inset shows the first 30-second interval of the

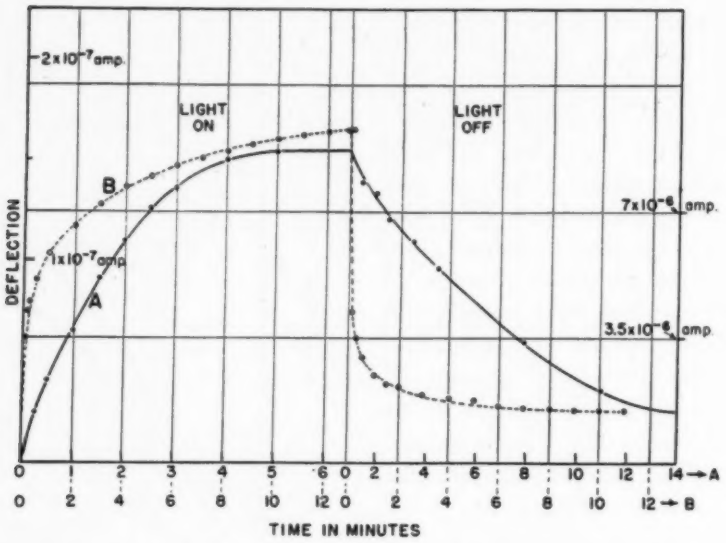

FIG. 4. (A) The rise and decay with time of the photo-currents in pure powdered lead chromate. The magnitude of the photo-current is indicated on the left axis. (B) Onset and decay of the photo-currents in a sintered pellet as a function of time. Current values are here indicated on the axis to the right. Note that the currents in the sintered pellet are a factor of 40 greater than the currents in the powdered sample.

225- and 1350-volt curves in greater detail with the intermediate plots omitted. It should be noted that there is a definite tendency toward saturation after the first 20 seconds of illumination. At the end of this relatively short period, the curve suddenly starts to rise with a sharper slope. The saturation time of this phenomena results from a consideration of the three types of observed photo-currents.[4] The electrons which are freed by the light quanta and make their way unhindered to the anode form what is known as the primary current. Not all the freed electrons, however, reach the anode. A great many of them may be trapped in various types of trapping centers from which they may be reexcited either thermally or optically into the conduction band. Electrons thus excited form a secondary current which is both time and voltage dependent. The curves in the inset of Fig. 3 represent the secondary currents superimposed upon the primary currents. The primary current is instantaneous and independent of the time of illumination. Owing to the finite time constants of the input circuit of the amplifier and the relative sizes of the primary and secondary currents, it is impossible to separate the former from the latter in the case of lead chromate.

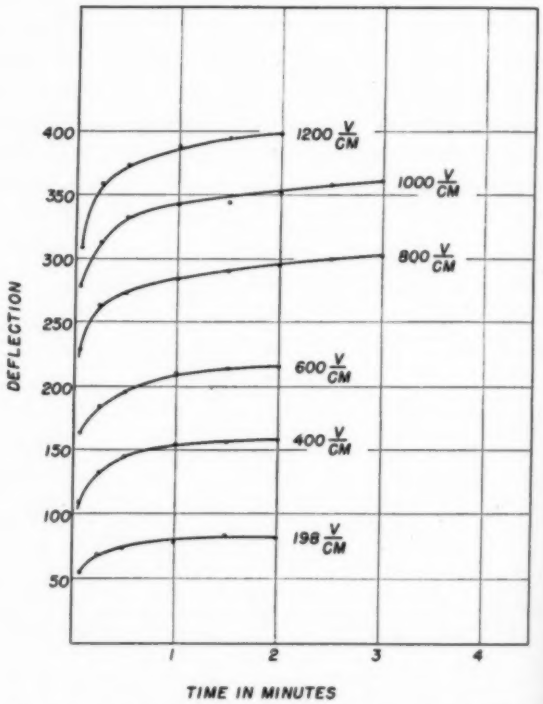

FIG. 5. Time dependence of photo-current for various fields in a sintered pellet. 100 scale divisions correspond to a current of 7×10^{-6} amp. This curve should be compared with the similar curve for powdered samples illustrated in Fig. 3.

[4] See F. Seitz, *Modern Theory of Solids* (McGraw-Hill, New York, 1940), Chapter XV.

The additional photo-current which rises sharply after the first 30 seconds of illumination may be due to additional electrons which enter the specimen from the cathode and move through it to the anode. This flow is induced by the space charge fields set up in the specimen by the migration of the primary and secondary electrons to the anode.[5] It should be expected that this current, too, would be time and voltage dependent, since the space charge fields are altered in virtue of the secondary photo-current. This explanation is further bolstered by an examination of the build-up and decay of the photo-currents as a function of time for a specified voltage. This dependence is illustrated by curve *A* in Fig. 4.

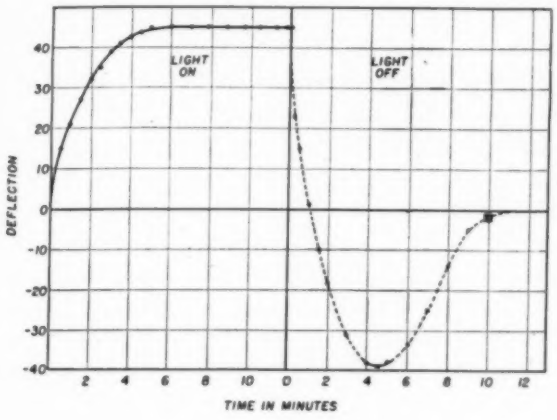

(a)

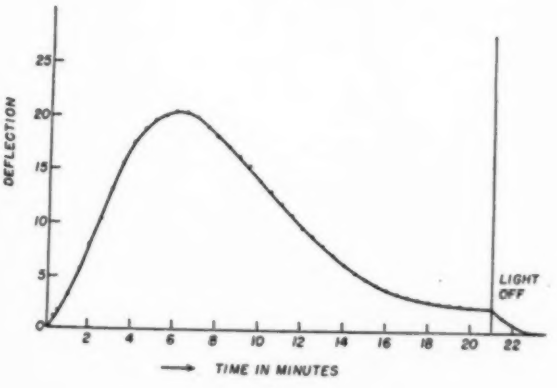

(b)

FIG. 6. Time dependence of the photoconductivity of impure lead chromate powders. (a) Shows the onset and decay for a powder which has been internally treated with impurities. It is seen that as the light is turned off there is a surge of current in the opposite direction tending to reduce the net dark current. (b) The same curve for material whose particle surfaces have been coated with impurities. In this case, polarization and grain boundary resistance tends to reduce the photo-current while the light is still on. Scale units are arbitrary.

[5] Reference 4, p. 569.

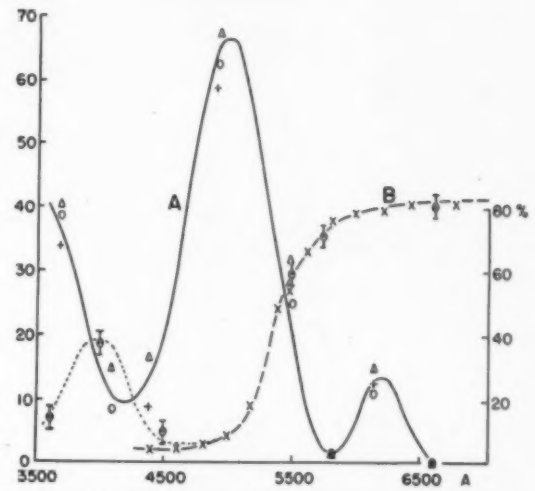

FIG. 7. (A) The spectral dependence of the photo-conductivity of lead chromate. The maximum at 5000A corresponds to a current of 5×10^{-3} amp/watt. (B) The spectral scattering lead chromate. The crosses are points obtained by Luckeish. The barred circles represent the results obtained in this laboratory. The ordinates on the right are the percent of scattered light.

In order to investigate the effect of grain density on the behavior of the photo-conductivity, a similar set of experiments were conducted on pressed pellets of $PbCrO_4$ sintered at 400°C. The density of such a sintered pellet closely approximates that of a single crystal and results from the union of the particles at the grain boundaries. In the case of a crystal the flow of electrons is unimpeded by grain boundaries and is limited only by thermal scattering and trapping. We may expect, therefore, that the current-time dependence of photo-conductivity in the powder will vary somewhat from that in the pellet. To investigate this effect, the photo-currents in the pill were studied as a function of time and voltage, the same as for the powder. The results are shown in Curve *B* of Fig. 4 and in Fig. 5. It is evident from these curves that there is no major difference between the behavior of a sintered pill and the pure powder. In both cases the secondary currents saturate due to the effects of trapping and space charge. The current rise, however, is much more rapid in the case of the sintered pellet. The time required to reach complete saturation varies from specimen and is presumably due to poor contact at the grain boundaries which may cause the flow of electrons

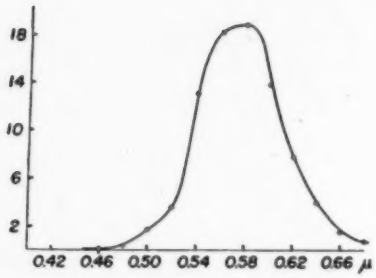

FIG. 8. The spectral reflectivity of lead chromate as viewed by the human eye. The scattering by the powder is multiplied by the spectral eye sensitivity to yield the illustrated curve. Ordinate units are arbitrary.

to cease before all the secondary electrons have been excited. That the resistance between grains is important is demonstrated by comparing the curves in Fig. 4 with similar curves, shown in Fig. 6, for lead chromate whose grains are coated with surface impurities. The most striking effect of the surface coating is the reduction of the photo-currents by a factor of approximately five. Furthermore, the onset and decay of the photo-conductivity varies considerably with the impurity. Both curves exhibit a behavior which can be explained by assuming that the space charge and resulting polarization in these specimens are greater than in the case of the pure material. Thus, for the material illustrated in Fig. 6A, the space charge causes a negative current to flow when the illumination is cut off. In the case illustrated in Fig. 6B, the polarization becomes so great that the secondary currents actually decrease upon continued illumination. Because of the increased resistance at the grain boundaries, the larger space charges in the case of the coated material are not unexpected.

The measurements of the spectral sensitivity of the photo-conductivity of lead chromate were made in much the same manner as the calibration previously described. The results are plotted as Curve *A* in Fig. 7 where the abscissa represents the wave-length of the incident light in angstrom units and the ordinates are the photo-currents referred to unit incident energy by means of corrected photo-cell readings. The peaks in the ultraviolet and the blue correspond to absorption bands observed in solutions of potassium chromate. Since the position of these bands would not be appreciably altered by the lattice, this may be considered as evidence that these bands are associated with the chromate ion. The corresponding photo-conductivity peaks may be interpreted as resulting from the excitation of electrons from the chromate ion from its fundamental bands into the conduction band or again as due to electrons excited from impurity centers by excitation waves produced by the interaction of the light with the chromate ions. It is doubtful, however, whether the peak in the red is also due to fundamental chromate ion absorption. It may possibly be due to absorption centers associated with interstitially placed positive ions or to foreign impurities. Evidence for this is discussed below.

The relative size of the various maxima is of considerable interest. To understand this more fully, it would be necessary to examine the ratio of photo-current to light absorbed rather than incident light. It will be seen that this is of considerable importance in interpreting the added peak in the red. In order, therefore, to obtain a qualitative indication of the shape of the absorption curve and to compare these results with the photo-conductivity data, experiments on the spectral scattering of the material were carried out. A carefully pressed $PbCrO_4$ surface was placed in the specimen mount in the position normally occupied by the inclined quartz plate. Thus the beam of the monochromatic light entering the chamber would be incident upon the

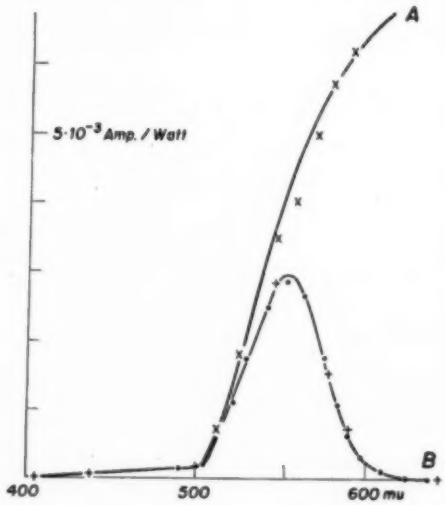

FIG. 9. Kapp's work on the spectral photo-conductivity of lead chromate. *A* represents the photo-conductivity referred to unit absorbed light whereas *B* is referred to unit incident light.

chromate surface at an angle of 45 degrees. The photo-cell then measures the light that is scattered down to it by the inclined surface. The data are referred to the same beam of light scattered from a perfectly white surface placed in an identical position. The curve resulting appears in *B*, Fig. 7 and is compared to a curve obtained by Luckiesh[6] in similar investigations on chrome yellow. It should be noted that there is a well-defined maximum in the neighborhood of 4000A. This maximum in scattering corresponds to the observed minimum of photo-conductivity in that region. The relatively high scattering in the red is probably associated with the fact that in this region the particle size approaches the order of magnitude of the wave-length of the incident light.

The scattering curve shows that the maximum scattering by lead chromate occurs in the red region of the spectrum. The yellow appearance of $PbCrO_4$ results from the spectral sensitivity of the eye. Thus the product of the scattering and the eye sensitivity is plotted in Fig. 8. This curve has a minimum in the yellow as expected.

On comparing the spectral photo-conductivity with the spectral scattering, it becomes evident that if we refer the relative photo-conductivity to the absorbed rather than the incident light, the height of the maximum in the red will be increased relative to the respective peaks in the blue and the ultraviolet. When the efficiency is calculated on this basis, the maxima in the red and the blue are more nearly equal. Assuming a 100 percent quantum conversion efficiency for the blue line, one may now calculate the mean displacement distance of the electrons. If I is the intensity of the absorbed radiation per unit distance between electrodes, the measured current i should be

$$i=\eta I e\omega/h\nu,$$

where $h\nu$ is the energy of the absorbed light quanta and ω is the mean displacement distance. η is the fraction of absorbed light quanta that free electrons, i.e., quantum efficiency.[7] The value of I is determined experimentally by comparing the thermopile deflection due to the blue line to that of a standard luminous source. It turns out

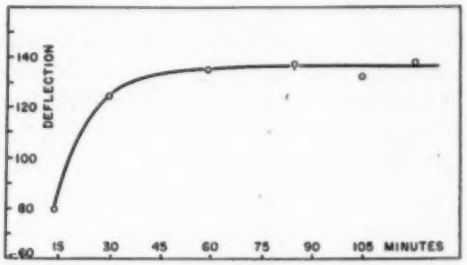

FIG. 10. Photo-conductivity in the red plotted as a function of time of illumination with ultraviolet light.

to be of the order of 1.45 ergs/cm/sec. The mean path calculated on this basis turns out to be approximately 3×10^{-3} cm.

It is interesting to compare this datum with the only other available datum on the photo-conductivity of lead chromate. The spectral photo-conductivity of single crystals of $PbCrO_4$ found by Kapp[8] is reproduced in Fig. 9. Referring conductivity to incident light intensity, Kapp finds a sharp maximum of photo-conductivity in the yellow which tapers off at greater wave-lengths until it finally approaches zero. This is in apparent contradiction to the results obtained in this laboratory. Although Kapp finds only one maximum, the authors find three. Moreover, Kapp finds the photo-conductivity rising sharply in precisely the same region that the writers find the curve approaching a minimum. The fact that Kapp worked with natural single crystals would seem to offer a possible explanation of this apparent contradiction. It is quite possible that natural single crystals contain sufficient impurities to mask the natural photo-conductivity of pure lead chromate.

The results of one further experiment indicate the possible explanation of the photo-conductivity in the red. A sample was alternately illuminated with ultraviolet light from a Hanovia lamp and with red light. The photo-conductivity in the red as a function of time of illumination with ultraviolet light was studied. These results appear in Fig. 10. It is seen that the red photo-current increases with time of illumination with ultraviolet. This experiment may be explained as follows. The illumination with ultraviolet light may free electrons from bound levels. Many of these freed electrons can now be trapped in higher empty levels presumably arising from impurities. These

[6] M. Luckiesh, J. Frank. Inst. **184**, 73 (1917).

[7] A detailed discussion appears in Seitz, reference 4, p. 565.

[8] G. Kapp, Ann. d. Physik **22**, 257 (1935).

trapped electrons can now be nearer the conduction band and may be excited to it by light of lower energy. As the exposure to ultraviolet light in increased, more electrons will be trapped in the higher impurity levels, and the photoconductivity in the red will increase. This increase will finally saturate when equilibrium is achieved between the number of electrons excited from the impurity levels into the conduction band and the number of electrons being retrapped.

It is the hope of the authors that the results of this investigation will be of material assistance in interpreting the spectral darkening of lead chromate which is now being studied by us in collaboration with A. H. Smith. The results of the latter investigation will be available shortly. A theoretical interpretation of the results of both these experiments will be presented by Dr. Frederick Seitz who initiated this program of research and whose active interest throughout the investigation was largely responsible for its completion.

In conclusion, the authors desire to express their indebtedness to the Krebs Pigments Department of the E. I. duPont de Nemours and Company for financial assistance in the form of a fellowship for one of us (J. E. G.) and for a plentiful supply of carefully prepared lead chromate, and to M. L. E. Chwalow who took an active part in the initial phases of the investigation.

PHYSICAL REVIEW VOLUME 64, NUMBERS 1 AND 2 JULY 1 AND 15, 1943

Intensity Anomalies and Perturbations in the CN Bands

A. T. WAGER*
Ryerson Physical Laboratory, University of Chicago, Chicago, Illinois
(Received April 1, 1943)

The rotational structures of the 0,0 violet and the 9,4 red CN bands, developed by $CHCl_3$ in active nitrogen, are measured on plates from the first and second orders of a 30-ft. grating. The rotational constants of the $b^2\Sigma, v=0$ and the $a^2\Sigma, v=4$ states are in good agreement with the previously published values; those for the $v=9\,^2\Pi$ state are $B'_9=1.5312\pm0.0008$ cm^{-1}, $D'_9=7.408\pm0.002\times10^{-6}$ cm^{-1}. The Λ-doubling in this state, except for four perturbations, can be represented by use of the constants $p_0=+0.01597$ and $q_0=-0.00080$. The value $\gamma'=+0.021$ is determined for the spin doubling in the $b^2\Sigma, v=0$ state. Four perturbations are found at $K=4$, 7, 11, and 15 for $b^2\Sigma$; extra P and R lines separated from the main lines by $\Delta\nu=-0.352$ cm^{-1}, $+0.938$ cm^{-1}, $+1.177$ cm^{-1}, and $+1.212$ cm^{-1}, respectively, appear in both the 0,0 and 0,1 bands of the violet system. In the red system, shifts of the right amount and direction in the lines $Q_1[3\frac{1}{2}]$, $R_1[7\frac{1}{2}]$, $P_1[7\frac{1}{2}]$, $R_2[10\frac{1}{2}]$, $P_2[10\frac{1}{2}]$, and $Q_2[15\frac{1}{2}]$ confirm the assumption that rotational levels of $^2\Pi, v=9$, perturb those of $b^2\Sigma, v=0$, and that the perturbations occur for the K and J values indicated. (Brackets denote upper state J.) The values of the perturbation matrix elements are obtained for the various levels. Some anomalies of the R branch band lines in the range 23–29 of K' values in the 0,0 violet band are mentioned.

The mechanism responsible for the enhancements of the main and extra lines of the 0,0 violet band is discussed. Collisions involving interstate transfer ($^2\Pi \rightarrow a^2\Sigma$) evidently occur, or are enhanced, at each perturbed level; and rapid redistribution of molecules among rotational levels by collisions must also occur. Where spin doublets are resolvable in the violet bands, rotational redistribution occurs without change of spin direction.

INTRODUCTION

Historical

IN 1928, G. Herzberg[1] reported that certain lines are enhanced in the emission of bands of the violet cyanogen system coming from the level $b^2\Sigma$, $v=0$, when excited by active nitrogen. The photographs were taken with a low dispersion instrument. Herzberg proposed fluorescence or collisions of the second kind as a tentative explanation. H. T. Byck,[2] in 1929, confirmed the experimental results; however, he found no evidence for a mechanism related to fluorescence, and therefore restricted the explanation to collisions of the second kind.

M. Fred, in 1932, photographed the above bands in the first order of a 21-ft. grating in this

* Now at Birmingham-Southern College, Birmingham, Alabama.

[1] G. Herzberg, Zeits. f. Physik **49**, 512 (1928).

[2] H. T. Byck, Phys. Rev. **34**, 453 (1929).

laboratory and obtained not only the enhancements mentioned, but also three extra lines in each branch. H. Beutler and M. Fred[3] explained this result by a detailed scheme of energy transfer. They compared the rotational terms of the $b^2\Sigma$, $v=0$ state with those of the $^2\Pi$, $v=9$ state as obtained by extrapolation. The calculations showed that four perturbations might be expected to occur, between $J=3\frac{1}{2}$ and $7\frac{1}{2}$ of $^2\Pi_{3/2}$, $v=9$ and $J=10\frac{1}{2}$ and $15\frac{1}{2}$ of $^2\Pi_{1/2}$, $v=9$ on the one hand, and $K=4$, 7, 11, and 15 in $b^2\Sigma$, $v=0$, on the other hand.

This hypothesis was subjected to an experimental test, a preliminary report of which was presented recently.[4] The description of the procedure and the derivation of the results form the content of this paper.

Excitation by Active Nitrogen

One of the ways to obtain the CN bands is to mix the vapor from carbon compounds with active nitrogen; a low-temperature flame yielding narrow rotational lines of low quantum numbers results from such a mixing. Many investigators[5–9] have worked with active nitrogen, either studying its properties or using it for exciting spectra from admixed gases. The excitation of the CN bands belongs to the second case; the CN is formed as a reaction product of the admixed gas with the active nitrogen. The molecules of this admixed gas must contain carbon atoms.

Active nitrogen itself is a mixture of inert and excited atoms and molecules of nitrogen, and its exact nature is not completely known.[10,11] Active nitrogen is formed in a discharge through nitrogen, especially by a spark discharge.

The detailed mechanism of the formation of active nitrogen is not completely known. It can be assumed that nitrogen atoms leave the discharge tube when the flow method is used, and that their recombination energy is the source for the excitation of any spectrum. This is in agreement with the long life of active nitrogen. Concerning the formation of the nitrogen atoms in the discharge, our knowledge of excitation processes by electron impact indicates that the direct dissociation of molecules is a rather rare process; therefore, it may be assumed that most of the nitrogen atoms are formed by collisions of two excited nitrogen molecules upon each other. The number of nitrogen molecules excited is proportional to the current density, and, if the cross section of the discharge tube is kept constant, to the current itself. If thus two excited molecules have to interact for the formation of atomic nitrogen, the concentration of atomic nitrogen will be proportional to the square of the current density. The assumption of such a mechanism explains the high efficiency of spark discharges compared to arc discharges in the formation of active nitrogen, as described in the following paragraphs.

The total power that can be impressed on a discharge tube depends on the construction of the tube, and especially on the size and cooling of the electrodes. The limit for constant load is usually given by the seals of the electrodes, occasionally by the softening of the Pyrex walls of the discharge tube. If the discharge is interrupted, then the momentary power input can be increased very much. If, for instance, the current is maintained over only about one-tenth of each cycle of the alternating current (five discharges during each 1/120 sec.), then the current density during this time can be increased approximately by the factor square root of ten; however, the yield of active nitrogen will be increased by a factor of ten with respect to the "steady" alternating current according to the assumption made above.

A further assumption made in this rough calculation is that the lifetime of the excited nitrogen molecules is not much longer than the time of such an interrupted discharge. The time of the spark discharge is of the order of 10^{-3} to 10^{-4} sec., and the lifetime of most kinds of excited molecules is less than 10^{-7} sec., hence such a

[3] H. Beutler and M. Fred, Phys. Rev. **61**, 107 (1942).
[4] A. T. Wager, Phys. Rev. **61**, 107 (1942).
[5] D. E. Debeau, Phys. Rev. **61**, 668 (1942), contains references to energy transfer phenomena in active nitrogen.
[6] Lord Rayleigh, Proc. Roy. Soc. **A176**, 1, 16 (1940). Both articles contain references to previous work.
[7] Reference 1.
[8] P. A. Constantinides, Phys. Rev. **30**, 95 (1927), contains references to E. P. Lewis, R. J. Strutt (Lord Rayleigh), F. Compte, Tiede, Pirani, Oosterhuies and Holst, H. W. Webb, H. A. Messenger, M. N. Saha, R. T. Birge, P. D. Foote, Ruark and Chenault, H. Sponer.
[9] J. Kaplan, Phys. Rev. **54**, 176 (1938); **61**, 202 (1942); Zeits. f. Physik **109**, 744, 750 (1938).
[10] H. Sponer, Zeits. f. Physik **34**, 622 (1925); Nature **117**, 81 (1926); and M. H. Hebb, Phys. Rev. **59**, 925 (1941).
[11] G. Cario and J. Kaplan, Zeits. f. Physik **58**, 769 (1929); also contains references to other work.

rough estimate is allowed. It is also assumed in this explanation that the mechanisms of excitation of the nitrogen molecule and of the formation of nitrogen atoms are the same during a spark discharge as during the period of an arc discharge, and that the difference in efficiency is caused only by the much different current densities.

EXPERIMENTAL PROCEDURE

The experimental problem was to develop a light source yielding CN bands of sufficient intensity to utilize the high dispersion and resolving power of the Ryerson 30-ft. circle grating spectrograph. This spectrograph permits one to obtain sufficiently precise wave-length measurements of the rotational lines in both bands for accurate measurements of the perturbations.

It was decided that the flow method[12] coupled with high energy input to the discharge tube offered the greatest probability of obtaining a CN flame of high intensity.

Experiments[13] have shown that most carbon compounds are satisfactory, but that the total intensity of the CN bands varies with the compounds used. Likewise, the relative intensities of the violet and red bands show wide variations. Since these effects are very likely caused by secondary processes of energy transfer in the reaction zone, they cannot be predicted, and it is necessary to compare the different compounds experimentally in order to discover the one which yields the CN bands with the greatest intensity. Gases investigated by the writer with respect to the red and violet CN bands were benzene, ethyl iodide, ethyl alcohol, ether, chloroform, carbon tetrachloride, acetone, ethyl acetate, benzaldehyde, pyridine, ethylene, aniline, and formaldehyde. The photographs in this preliminary study were made with a Hilger E-3 quartz spectrograph. The carbon compound finally selected was chloroform, which gave the greatest intensity in both the red and the violet bands. (Pyridine and carbon tetrachloride gave CN bands which were but slightly weaker than those obtained with chloroform.)

The electrical energy was furnished by a 25,000-volt transformer whose load was regulated by inductances in the primary. The power input varied from 1.5 to 4.5 kva. Power of 2.0 to 2.5 kva was used for the long exposures. Four condensers, in series, of total capacity 0.0025μf, were charged by the transformer and allowed to discharge across a discharge tube in series with a spark gap of about 2-cm separation traversed by a strong air blast. The combined action yielded 3 to 5 sparks during each half-cycle of the alternating current. A heavy grounded wire was connected to the grounded side of the a.c. input, one side of the transformer secondary, one side of the condensers, the discharge tube electrode nearer the pump, the transformer case, the condenser cases, the motor and pump frames, the supporting framework of the apparatus, and the hardware cloth used to protect the power unit.

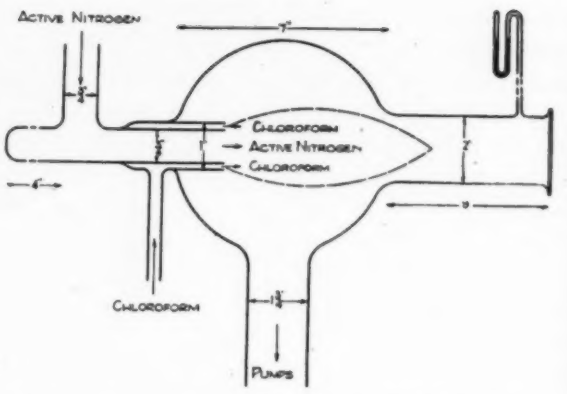

FIG. 1. Afterglow bulb for mixing $CHCl_3$ vapor and active nitrogen issuing separately as indicated from two concentric glass tubes. The resulting flame is photographed through the quartz window fastened by Picein to the end of the nine-inch tube.

The discharge tube finally adopted was made of one-inch Pyrex tubing with two sealed-in 150-mil tungsten rods, protected by shorter Pyrex sleeves fastened to the seal. The distance between the electrodes was eight inches. The tube and electrodes were cooled by strong air blasts.

The afterglow tube was made from a two-liter Pyrex bulb (Fig. 1). On one side was sealed a piece of two-inch tubing nine inches long to which a quartz window (two and one-quarter inches in diameter) was fastened by Picein to a flange. Diametrically opposite this window there were two concentric tubes cut off even with each other; the outer tube introduced the chloroform from its container. The active nitrogen and the chloroform vapor mixed as they issued separately

[12] Cf. R. S. Mulliken, Phys. Rev. **26**, 1 (1925).
[13] See references 5–9.

from the concentric tubings and gave a flame which varied from four to eight inches in length, depending on the pressure, relative amounts of the two components, and the power. The flame was directed toward the quartz window, mentioned above, through which the light was photographed. Stray light caused by internal reflections of the light from the discharge tube along the glass tubes was minimized by a set of Rayleigh's horns along the duct of active nitrogen, and light shields were placed externally where necessary.

It was found by experiment that the amount of active nitrogen formed in the discharge tube was so great that a high pumping speed was necessary to utilize it in the afterglow bulb. Two Megavac pumps in parallel were connected to the afterglow bulb by tubing one and three-quarter inches wide, with wide protecting traps cooled by dry ice in acetone, one for each pump.

Tank nitrogen was found to be sufficiently pure for this problem. It was admitted to the discharge tube through a mercury flowmeter and a small stopcock to control the rate of flow, which was about thirty liters per hour. The chloroform vapor was admitted to the mixing tube through a stopcock in a side tube and was used up at the rate of about one cc of liquid per hour. The pressure in the afterglow tube was kept at 4–12 mm mercury. At lower pressures, stray discharges were formed from the discharge tube all the way to the pumps. The flame spectrum then showed admixture of nitrogen bands. The flame was focused on the grating spectrograph by crossed cylindrical lenses in order to give maximum intensity on the plates. A careful check was kept on both the barometric pressure and the temperature of the grating room, so as to forestall any false shifts in the lines. A slit width of 15μ was the minimum used, and 25μ the maximum.

Two 30,000 lines/inch gratings, called No. 2 and No. 3, each with 150,000 lines exposed, mounted on the same circle and using the same slit, were available for this problem. Exposures of the CN bands were made with each grating, as follows for the individual bands: No. 3, λ5598 of the red system, 1st order; λ4216 of the violet system, 1st order; and λ3883 of the violet system, 1st and 2nd orders; No. 2, λ5598, 1st order; λ4216, 1st order; and λ3883, 1st order. The band λ4216 was very weak in 2nd order, and no lines pertaining to λ3593 were obtained with this spectrograph. Eastman Process plates were used for λ3883, 1st and 2nd orders; Eastman 33 plates for λ4216; and Eastman 103-D plates sensitized with ammonia for λ5598.

λ3883, 1st order, could be photographed in one and one-half hours; exposures to 8 or 12 hours brought out the underlying (1,1), (2,2), and (3,3) bands. λ4216, 1st order, required at least eight hours to obtain a strong picture. λ3883, 2nd order, was photographed for a time-period not less than eight hours, and λ5598, 1st order, required at least ten hours.

The standard iron arc was used to calibrate the plates; the iron standards and the band lines were measured with a Geneva comparator. All wave-lengths were reduced to wave numbers in vacuum with the aid of Kayser's "Tabelle der Schwingungzahlen."

DESCRIPTION AND ANALYSIS OF THE DATA

The two plates, one of the 9,4 red band and one of the 0,0 violet band, on which the frequency data reported later are based, were obtained with the No. 3 grating. Both bands were photographed during a single exposure taken with a pressure of about 3–4 mm in the mixing bulb. Other plates, obtained during different exposures, were also measured and the results reported later were checked against these to insure accuracy.

The 0,0 Violet Band

The CN $^2\Sigma(0,0)$ band was measured some years ago by Uhler and Patterson[14] under fairly high dispersion using a carbon arc source, and the wave numbers calculated from their data are given by Herzberg.[15] New measurements made on the second-order plate, with a dispersion of 0.368A/mm, yield essentially the same formula as that given by Herzberg;[15] the equation for the band lines obtained from the present measurement is:

$$\nu = 25{,}797.848 + 3.850m + 0.06796m^2 - 0.000026m^3 - 0.00000022m^4, \quad (1)$$

[14] Uhler and Patterson, Astrophys. J. **42**, 434 (1915).

[15] G. Herzberg. *Molecular Spectra and Molecular Structure, I. Diatomic Molecules* (Prentice-Hall, Inc., New York, 1939), pp. 44–46.

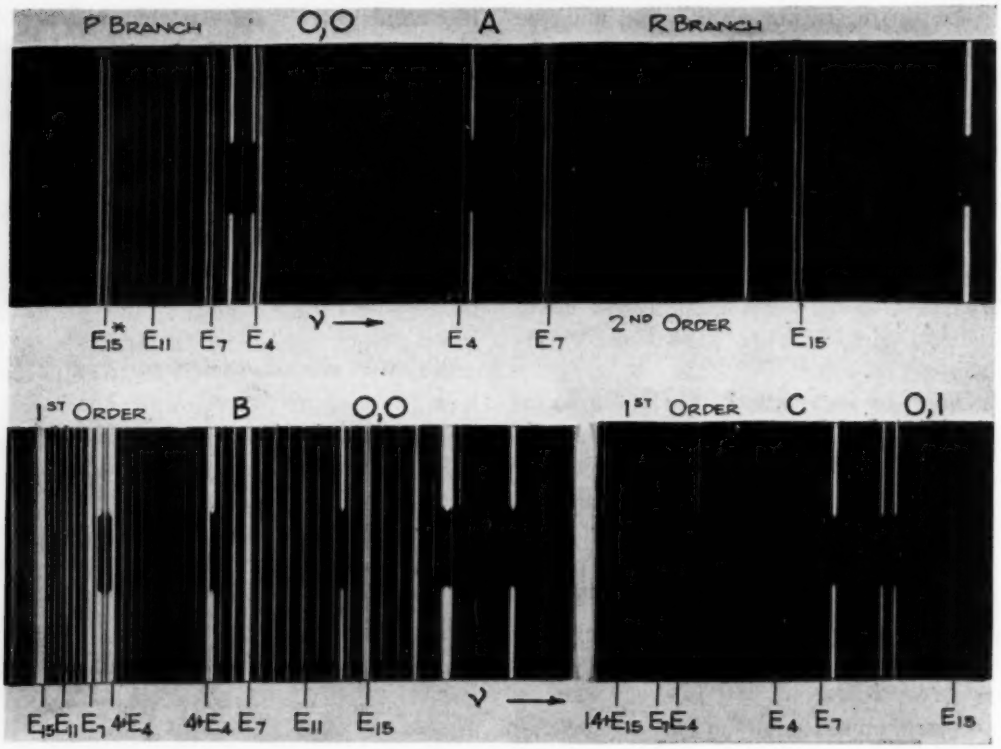

FIG. 2. Bands of the violet CN system. *A*. The 0,0 violet band, second order. The branches are indicated above. Below, four extra lines in the *R* branch and three in the *P* branch are marked. *B*. The 0,0 violet band, first order, over-exposed. Extra lines are marked as in *A*. E_{11} is strong in each branch. The underlying bands of 1,1 and 2,2 violet appear here. *C*. The 0,1 violet band, first order. E_{11} is not visible in enlargement, but appears as very weak line on plate. E_{15} blends with $K'(14)$ in *P* branch. Enhancements of the perturbed lines and the extra lines are apparent in both *A* and *C*. The plates from which these enlargements were made were photographed during the same exposure, with a pressure of 3–4 mm in the afterglow bulb.
* Upper state numbering is used throughout.

where ν refers to centers of doublets. In addition to the lines represented by this formula, the plate shows clearly the four extra lines expected at $K'=4$, 7, 11, and 15 in the *P* as well as in the *R* branch. The separations of these extra lines from the main lines at $K'=4$, 7, 11, and 15 were $\Delta\nu=-0.352$ cm^{-1}, $+0.938$ cm^{-1}, $+1.177$ cm^{-1}, and $+1.212$ cm^{-1}, respectively. Measurements made on other first- and second-order plates of the (0,0) band are in agreement.

Further proof that the perturbed levels belong to the upper state of the 0,0 transition appears in photographs of the 0,1 (λ4216) transition, which show the four extra lines at the same separations from the proper K' band lines in both branches.

The relative intensities of the perturbed and extra lines are dependent on the pressure in the mixing chamber of the apparatus. At high pressures of nitrogen, 8 mm of Hg or greater, the extra lines are relatively weak, and the perturbed lines are not much stronger than the other lines of the band; the extra line at $K'=11$ is too faint to be seen with certainty. If the pressure is lower, 3–4 mm, the extra lines and the perturbed lines are both intensified (see Fig. 2), in both bands λ4216 and λ3883. The extra line at $K'=11$ is now unmistakably present, although still much weaker than the other three. It is quite strong on over-exposed first-order plates of the 0,0 band, as can be seen in Fig. 2 (4–8 hr. exposure).

A study of the 0,0 violet band photographed in second order shows that the lines of the band are sharp and single to $K'=7$. They appear slightly diffuse from $K'=7$ to $K'=15$, and are clearly resolved doublets of unequal intensity above $K'=15$. The doublet separation is very nearly constant in the measurable range (to $K'=22$ in the *P* branch and $K'=20$ in the *R*

branch), the average separation being

$$\Delta\nu = 0.211 \pm 0.012 \text{ cm}^{-1}.$$

The lines with higher K' values in the R branch of the 0,0 violet band (on first-order plates) show anomalous intensities and doublings for values of K' from 22 to 29. All the doublets from $R(16)$ through $R(21)$ are strong and well-resolved; $R(22)$ is barely resolved; $R(23)$ is weak and just resolved; $R(24)$ consists of two components of equal intensity; $R(25)$ looks like a broad asymmetrical unresolved line; $R(26)$ is just resolved into two components of equal intensity and is much weaker; $R(27)$ is strong, broad, and unresolved; and $R(28)$ and $R(29)$ consist of well-resolved components of unequal intensity. Lines with higher values of K' are obscured and partly blended with the lines of the underlying 2,2 and 3,3 bands. These effects cannot be checked on the P branch because the head is formed in this region of K'. A comparison with higher K' members of the 0,1 band was not possible because $K'=21$ was the last one that was obtainable with measurable intensity.

To explain these anomalies, a study of perturbations possible in this region was made. The terms of the $a^2\Sigma$, $v=14$ state lie near the $b^2\Sigma, v=0$ terms; a graph in which extrapolated B_v values of the terms of these two systems are plotted against $K(K+1)$ showed that the term-curves cross at about $K=34$. The energy difference at the K values mentioned above is still approximately 200 cm^{-1}, a value too large to explain the observed anomalies on the basis of the usual type of rotational perturbation. There may be secondary processes which cause this effect; to investigate it may require that one mix different substances with the active nitrogen and operate the mixing tube at different pressures. It is also possible that blends with the underlying 1,1, 2,2, or 3,3 bands may account for these anomalies. Photographs of the 0,0 violet bands with a stronger light source and with greater dispersion would be necessary to check this possibility.

The 9,4 Red Band

The rotational structures of several red bands of cyanogen [(4,1), (5,2), (6,1), (6,2), (7,2), (7,3), and (8,3)] were measured in 1932.[16] The method of analysis used in that report was adopted in the study of the $^2\Pi - {}^2\Sigma$ 9,4 band, whose upper level is the cause of the perturbations mentioned earlier in the $^2\Sigma - {}^2\Sigma$ 0,0 band. The $^2\Pi$ state is an inverted one intermediate between case a and case b. The following branches appear in emission:

$^2\Pi_{3/2}$ to $^2\Sigma$: $R_1(J)$; $Q_1(J)+{}^QR_{12}(J)$;
$P_1(J)+{}^PQ_{12}(J)$; and ${}^OP_{12}(J)$;
$^2\Pi_{1/2}$ to $^2\Sigma$: ${}^SR_{21}(J)$; $R_2(J)+{}^RQ_{21}(J)$;
$Q_2(J)+{}^QP_{21}(J)$; and $P_2(J)$.

In this band the ${}^SR_{21}$ and the ${}^OP_{12}$ branches are weak but measurable, but the satellite branches are not resolved from the main branches. Eight branches, therefore, were measured and analyzed for this band.

Table I contains the wave numbers in vacuum of the measured lines of the branches of this band and of the differences between the measured frequencies and the calculated frequencies ($\nu_{obs} - \nu_{calc}$), based on the constants given below.

The wave numbers of the lines were calculated as the differences between the terms of the $^2\Pi$ and the $^2\Sigma$ levels, each being determined separately. The following equations, the constants of which were obtained as described below, yielded the term values used.

$$\begin{aligned}
^2\Pi_{3/2}:\ T'_{1d}(J) &= 26{,}872.810 \\
&\quad +1.5312\{(J+\tfrac{1}{2})^2-1 \\
&\quad -\tfrac{1}{2}[4(J+\tfrac{1}{2})^2-1{,}267.627]^{\frac{1}{2}}\} \\
&\quad -7.408\times10^{-6}J^4, \\
^2\Pi_{1/2}:\ T'_{2d}(J) &= 26{,}872.810 \\
&\quad +1.5312\{(J+\tfrac{1}{2})^2-1 \\
&\quad +\tfrac{1}{2}[4(J+\tfrac{1}{2})^2-1{,}267.627]^{\frac{1}{2}}\} \\
&\quad -7.408\times10^{-6}(J+1)^4, \qquad (2) \\
^2\Sigma:\quad T''_1(J) &= 9{,}042.415 \\
&\quad +1.8202J^2+0.003(J-\tfrac{1}{2}) \\
&\quad -6.44\times10^{-6}J^4, \\
^2\Sigma:\quad T''_2(J) &= 9{,}042.415+1.8202(J+1)^2 \\
&\quad -0.003(J+\tfrac{1}{2}) \\
&\quad -6.44\times10^{-6}(J+1)^4.
\end{aligned}$$

The rotational constants for the $b^2\Sigma$, $v=0$ and $a^2\Sigma$, $v=4$ states were determined by plotting

[16] Jenkins, Roots, and Mulliken, Phys. Rev. 39, 16 (1932).

TABLE I. Wave numbers* of the lines of the 9,4 band.

J'	R_1	ν(obs.) $-\nu$(calc.)	P_1	ν(obs.) $-\nu$(calc.)	Q_1	ν(obs.) $-\nu$(calc.)	$^qP_{12}$	ν(obs.) $-\nu$(calc.)
1½	17,807.157	+0.053	17,796.166	−0.011	17,803.512	+0.051	17,785.130	(−0.142)
2½	810.956	+0.052	792.755	+0.058	803.666	+0.045	778.350	(+0.191)
3½	814.104	+0.060	788.607	+0.049	*p* 803.128	+0.004	*p* 770.759	(+0.370)
4½	816.566	+0.045	783.820	+0.064	802.017	+0.053	762.267	(+0.309)
5½	818.413	+0.066	778.350	+0.045	800.201	+0.046		
6½	819.585	+0.066	772.281	+0.079	797.727	+0.032	743.077	−0.077
7½	*p* 820.204	+0.161	*p* 765.662	+0.208	794.615	+0.026	733.035	(+0.253)
8½	819.942	+0.021	758.071	+0.011	790.875	+0.033	721.754	−0.018
9½	819.128	−0.031	750.048	+0.019	786.459	+0.005	710.264	+0.048
10½	817.756	−0.003	741.372	+0.006	781.436	−0.002		
11½	815.723	−0.002	732.079	+0.011	775.766	−0.022	$^qP_{12}$ lines very weak.	
12½	813.068	+0.007	722.141	−0.005	769.464	−0.051		
13½	809.763	−0.006	711.582	−0.056	762.570	−0.049		
14½	805.838	−0.018	700.355	−0.055	755.051	−0.055		
15½	801.277	−0.041			746.897	−0.076		
16½	796.166	−0.001			738.144	−0.089		
17½	790.130	−0.015			728.777	−0.101		
18½	784.002	−0.006			718.734	−0.128		
19½	777.019	+0.007			708.190	−0.159		

J'	R_2	ν(obs.) $-\nu$(calc.)	P_2	ν(obs.) $-\nu$(calc.)	Q_2	ν(obs.) $-\nu$(calc.)	$^sR_{21}$	ν(obs.) $-\nu$(calc.)
½			( )	( )	17,853.528	−0.070		
1½	17,858.284	−0.043	(17,840.326)	(+0.194)	850.971	−0.049	17,861.801	(−0.224)
2½	858.937	+0.021	833.384	−0.058	847.928	−0.029	866.153	+0.007
3½	858.937	−0.034	826.270	+0.014	844.343	−0.056	869.871	+0.010
4½	858.580	+0.008	818.555	−0.023	840.326	−0.020	873.113	+0.032
5½	857.677	−0.022	810.365	−0.029	835.753	−0.019	875.801	−0.004
6½	856.270	−0.016	801.713	+0.004	830.705	−0.025	877.943	−0.062
7½	854.357	−0.004	792.518	+0.006	825.173	+0.010	879.688	−0.016
8½	851.937	+0.013	782.804	−0.002	819.128	+0.043	880.903	+0.011
9½	848.982	+0.017	772.590	+0.006	812.510	+0.018	881.572	+0.010
10½	*p* 845.531	+0.049	*p* 761.862	+0.024	805.402	+0.024	881.805	+0.105
11½	841.522	+0.048	750.603	+0.032	797.727	−0.014	881.370	+0.045
12½	836.973	+0.042	738.829	+0.055	789.608	+0.031	880.504	+0.090
13½	831.932	+0.079	726.498	+0.056	780.928	+0.047	879.023	+0.057
14½	826.302	−0.039	713.648	−0.029	771.722	−0.023	877.099	+0.022
15½	820.204	+0.140	700.355	+0.183	*p* 762.267	+0.411	*p*	
16½	813.490	+0.148	686.300	+0.079	751.592	+0.031	871.647	+0.281
17½					740.764	+0.069		
18½					729.374	+0.100		
19½								

* Estimated error = ±0.015 cm^{-1}.
p denotes perturbed lines.

$\Delta_2F/(4J+2)$ against $(J+\frac{1}{2})^2$.[17] The slope of the resulting straight line yields $2D_v$, and the intersection with the ordinate axis gives B_v.

This method, however, does not apply equally well for the $^2\Pi$ state because the rotational formula is more complicated on account of the transition of the coupling from case *a* to case *b* within the range of observed low rotational terms. Therefore, the procedure described below was adopted. Formulas for $\Delta_2F'_1(J)$ and $\Delta_2F'_2(J)$ were obtained from Eq. (2) and then added; the formula which results for the $^2\Pi$ state is

$$[\Delta_2F'_{1d}(J)+\Delta_2F'_{2d}(J)]/(4J+2) = 2B'_v+4D'_v(J^2+J+2).$$

The quantity on the left of this equation when plotted against (J^2+J+2) yields a straight line whose intersection with the ordinate axis is $2B'_v$ and whose slope is $4D'_v$. $B'_9=1.5312\pm0.0008$ cm^{-1} and $D'_9=7.408\pm0.002\times10^{-6}$ cm^{-1} were the values thus obtained for the rotational constants of the $^2\Pi$, $v=9$ state.

[17] Reference 15, p. 191–204.

The experimental value of A, the separation of the electronic $^2\Pi$ sub-levels, was determined from the relation[18]

$$A = T'_2(\tfrac{1}{2}) - T'_1(1\tfrac{1}{2}) + B'_v - 3B'^2_v/A. \quad (3)$$

The numerical value obtained is $A_9 = -51.41$ cm^{-1}, in line with those given earlier for the red cyanogen bands, as follows:[19]

$$A_4 = -52.14 \text{ cm}^{-1}, \quad A_5 = -52.33 \text{ cm}^{-1},$$
$$A_6 = -52.52 \text{ cm}^{-1}, \quad A_7 = -50.89 \text{ cm}^{-1},$$

and

$$A_8 = -51.65 \text{ cm}^{-1}.$$

Λ-Doubling

The Λ-doublings in the $^2\Pi$ states are defined as differences in term value of sub-levels with equal J values, as follows:

$$\Delta\nu_{dc} = T_d(J) - T_c(J),$$

the subscripts c and d having the significance assigned to them by Mulliken.[20] The magnitudes of the doubling can be evaluated from the differences of observed band lines, as follows:

$$^2\Pi_{1/2}: [R_2(J) - Q_2(J)] - [Q_2(J+1) - P_2(J+1)] \sim 2\Delta\nu_{2dc}(J+\tfrac{1}{2}), \quad (4)$$
$$^2\Pi_{3/2}: [R_1(J) - Q_1(J)] - [Q_1(J+1) - P_1(J+1)] \sim 2\Delta\nu_{1dc}(J+\tfrac{1}{2}).$$

The theoretical expressions for the Λ-doubling for cases intermediate between case a and case b are as follows:

$$\Delta\nu_{2dc} = [(\tfrac{1}{2}p_0 + q_0)(1 + 2X^{-1} - YX^{-1}) + 2q_0X^{-1}(J-\tfrac{1}{2})(J+1\tfrac{1}{2})](J+\tfrac{1}{2}), \quad (5)$$
$$\Delta\nu_{1dc} = [(\tfrac{1}{2}p_0 + q_0)(-1 + 2X^{-1} - YX^{-1}) + 2q_0X^{-1}(J-\tfrac{1}{2})(J+1\tfrac{1}{2})](J+\tfrac{1}{2}),$$

where $Y = A/B_v$, $X = |[Y(Y-4) + (J+\tfrac{1}{2})^2]^{\frac{1}{2}}|$, and p_0 and q_0 are coefficients independent of J which are characteristic of the particular electronic and vibrational state. The constants obtained from the data for $v' = 9$ were: $p_0 = +0.01597$ and $q_0 = -0.00080$. Figure 3 shows the comparison between the observed and calculated values of $\Delta\nu_{idc}$ for the initial state $v' = 9$. A study of the graph shows that the observed values of $\Delta\nu_{idc}$'s exhibit large deviations around the J numbers where perturbations occur. The $\Delta\nu_{idc}$'s obtained from this graph were used in evaluating T'_{1c} and T'_{2c} by adding $\Delta\nu$'s to T'_{1d} and T'_{2d} as given by Eq. (2).

Perturbations

It was stated earlier that four extra lines appear in the P and R branches of the 0,0 band of the violet system, and that a calculation performed by Beutler and Fred,[3] using constants for the $^2\Pi$, $v = 9$ state obtained by extrapolation, had indicated that the perturbation was caused by the levels of the latter. The just-obtained analysis of the $^2\Pi$, $v = 9$ state confirms this conclusion, as will be shown quantitatively.

The terms of the $b^2\Sigma$, $v = 0$ state were calculated and compared with those of the $^2\Pi$ state. The graph in Fig. 4, with $J(J+1)$ values as abscissae and T values as ordinates, shows the $^2\Sigma$ state broken into its two components, with J equal to $(K+\tfrac{1}{2})$ and $(K-\tfrac{1}{2})$, and the states $^2\Pi_{3/2}$ and $^2\Pi_{1/2}$. In this diagram each sequence of rotational levels forms very approximately a straight line, and there are four points of intersection, close to $J' = 3\tfrac{1}{2}$, $7\tfrac{1}{2}$, $10\tfrac{1}{2}$, and $15\tfrac{1}{2}$.

Each of these J values is the crossing point of two sub-levels, and the correlation is as follows (see Table II).

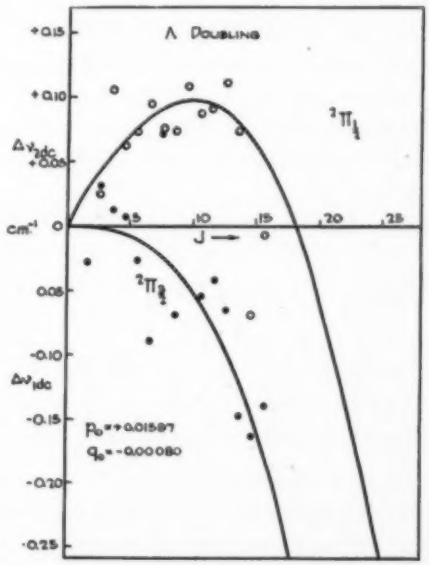

FIG. 3. Λ-doubling in the $^2\Pi$, $v = 9$ state. The heavy lines are the theoretical curves obtained with the coefficients given. The circles represent the values of $\Delta\nu_{2dc}(^2\Pi_{1/2})$ obtained from the main branches; the dots the values of $\Delta\nu_{1dc}(^2\Pi_{3/2})$ obtained similarly.

[18] R. S. Mulliken, Phys. Rev. **33**, 747 (1929).
[19] Reference 16, p. 32.
[20] R. S. Mulliken, Rev. Mod. Phys. **3**, 94 (1931).

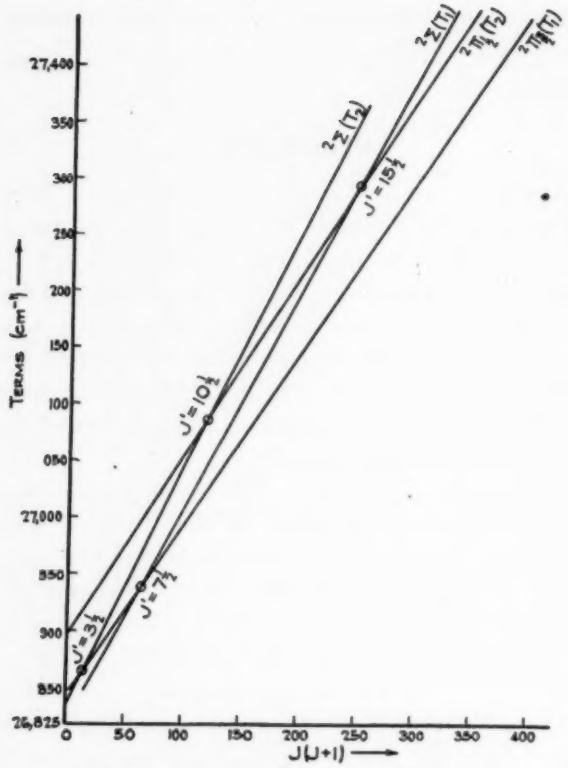

FIG. 4. Curves showing crossing points of terms of $b^2\Sigma$, $v=0$ and of $^2\Pi_{3/2}$ and $^2\Pi_{1/2}$. The $^2\Sigma$ state is broken into its two components, $(K+\frac{1}{2})$ and $(K-\frac{1}{2})$. The four points of intersection are close to $J'=3\frac{1}{2}$, $7\frac{1}{2}$, $10\frac{1}{2}$, and $15\frac{1}{2}$.

The respective parities of the perturbing levels are designated in the sixth column of Table II. In $^2\Sigma$, only one of the two neighboring sub-levels associated with a given K and having equal parity, but which have $J=K+\frac{1}{2}$ or $K-\frac{1}{2}$, will be perturbed. In $^2\Pi_{1/2}$ or $^2\Pi_{3/2}$, however, only one of the two component levels, differing in parity, of the Λ-doublet belonging to a given J will be perturbed. The band lines involving these $^2\Pi$ sub-levels are found in various branches of the 9,4 red band, as follows (cf. Fig. 4):

$^2\Pi_{3/2}$, $J'=3\frac{1}{2}$ (parity +): $Q_1[3\frac{1}{2}]$, $^OP_{12}[3\frac{1}{2}]$,
$J'=7\frac{1}{2}$ (parity −): $R_1[7\frac{1}{2}]$, $P_1[7\frac{1}{2}]$,
$^2\Pi_{1/2}$, $J'=10\frac{1}{2}$ (parity −): $R_2[10\frac{1}{2}]$, $P_2[10\frac{1}{2}]$,
$J'=15\frac{1}{2}$ (parity −): $Q_2[15\frac{1}{2}]$, $^SR_{21}[15\frac{1}{2}]$.

Note: [ ] denote upper state J.

The observations in the satellite branches $^OP_{12}$ and $^SR_{21}$ suffer from lack of intensity. For the other branches, given above, Table I shows that the $\nu_{obs}-\nu_{calc}$ is greater for these lines than for their neighbors, indicating the existence of perturbations.

The differences of the calculated unperturbed terms between $^2\Pi_{3/2}$ and $^2\Sigma$, and $^2\Pi_{1/2}$ and $^2\Sigma$, respectively, are given in column seven of Table II.

The smaller the energy difference between the unperturbed levels (column seven, Table II), the larger, other things being equal, the perturbation that is to be expected and the larger in wave mechanics the mixing of the unperturbed eigenfunctions. The observable results expected from mixing are shifts of the levels and the sharing of transition probabilities between the two states which mix. For a 50 percent mixing, the two levels will exhibit equal probabilities in all their transitions. Extra band lines may appear, whose relative intensities should be a measure of the amount of perturbation.

These viewpoints may first be applied qualitatively to the band lines and extra lines in the violet bands. The value ΔT for $J'=10\frac{1}{2}$ is the largest in Table II, and the connected perturbation is the weakest; this agrees with the experiments (see above). The perturbations at $J'=3\frac{1}{2}$ and $7\frac{1}{2}$ are moderately strong. The perturbation at $J'=15\frac{1}{2}$ is the strongest, as expected, because here the two perturbing levels are moderately close together at a large value of J. In all cases, the extra lines are weaker than the regular lines, indicating that the perturbation never reaches the value of 50 percent mixing in the eigenfunctions.

TABLE II. Unperturbed terms of $b^2\Sigma$, $v=0$, and $^2\Pi$, $v=9$ (cm^{-1}), based on Eq. (1) for $^2\Sigma$ and Eq. (2) for $^2\Pi$.

J	$^2\Sigma(T_2)$	$^2\Sigma(T_1)$	$^2\Pi_{1/2}(T_2)$	$^2\Pi_{3/2}(T_1)$	Parity	$T(^2\Pi)-T^2(\Sigma)$
$3\frac{1}{2}$	26,868.167			26,867.844	+	−0.323
$7\frac{1}{2}$		26,938.673		26,939.368	−	+0.695
$10\frac{1}{2}$	27,087.461		27,088.466		−	+1.005
$15\frac{1}{2}$		27,298.763	27,299.315		−	+0.552

For the $^2\Pi$, $v=9$ levels it is expected that there will be corresponding shifts and extra lines. The shifts are apparent for the lines $Q_1[3\frac{1}{2}]$, $R_1[7\frac{1}{2}]$, $P_1[7\frac{1}{2}]$, $R_2[10\frac{1}{2}]$, $P_2[10\frac{1}{2}]$, and $Q_2[15\frac{1}{2}]$. They confirm completely the perturbations at $K'=4$, 7, 11, and 15 in the violet bands, in that the shifts are in the direction opposite to those in the $b^2\Sigma$, $v=0$ levels, and the term values of the upper levels of the extra lines in $b^2\Sigma$ agree fairly well with those of the $^2\Pi$ system (see Table III).

Exact agreement should exist if all formulas and measurements had been exact. However, the extra lines were not observed in the red band in the intensity expected from analogy with the violet band. The intensity of the red band is rather low, so that variations in intensity would be difficult to determine.

Most of the expected perturbed lines in the 9,4 band were near the heads of the branches to which they belong, or else in a group of other lines which would obscure them. The only line lying isolated is $R_2[10\frac{1}{2}]$, which is the least perturbed; there is no apparent weakening of this line, and no extra line is discernible. If an extra line exists, it would be blended with $Q_2[3\frac{1}{2}]$, as may be shown by calculation. Examination of $Q_2[3\frac{1}{2}]$ under high magnification shows indications of doubling, but considerations below suggest the blended extra line is not really the $R_2[10\frac{1}{2}]$ companion. The corresponding line in the P_2 branch has no measured line in the position where the extra line is expected. $Q_1[3\frac{1}{2}]$ is in the head of the Q_1 branch, and if any extra line were there, it would be completely lost. $R_1[7\frac{1}{2}]$ lies near the head of the R_1 branch, and no conclusion may be drawn, for any extra line would be mixed with $R_1[9\frac{1}{2}]$. $P_1[7\frac{1}{2}]$ is shifted but no extra line is found. $Q_2[15\frac{1}{2}]$, which should be perturbed the most and should give the strongest extra line, is shifted the most, as stated above; however, again no line could be identified definitely as an extra line.

Theory states that a small residual shift occurs in those levels immediately preceding and following the perturbed level when perturbations occur between two rotational levels. To check this quantitatively, a study of the 0,0 violet band was made; this band, as stated earlier, shows the enhancements and extra lines much more strongly than does the 9,4 red band. Figure 5

TABLE III. Term values* of upper levels of extra lines in 0,0 violet and of main lines in 9,4 red (cm^{-1}).

From $^2\Sigma$ data	From $^2\Pi$ data
26,867.838 (T_2)	26,867.804 (T_1)
26,939.522 (T_1)	26,939.553 (T_1)
27,088.629 (T_2)	27,088.491 (T_2)
27,299.781 (T_1)	27,299.740 (T_2)

* These values were obtained by adding $\nu_{obs}-\nu_{calc}$ from Fig. 6 for $^2\Sigma$ or from Table I for $^2\Pi$ data differences to the calculated unperturbed terms of Table II, and for $^2\Sigma$ also adding the observed interval Δ from main to extra line.

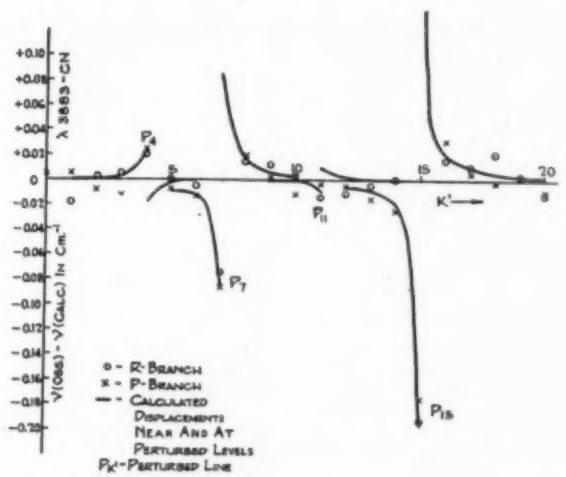

FIG. 5. Graph showing $\nu_{obs}-\nu_{calc}$ for the 0,0 violet band; ν_{calc} is obtained from Eq. (1), adjusted for γ' (see text). Circles represent $\Delta\nu$'s for the R branch, crosses for the P branch. The perturbed lines at $K'=4$, 7, 11, and 15 are indicated by $P_{K'}$. The heavy curves represent the calculated shifts in $\Delta\nu$ near and at each perturbation, given by $\frac{\delta}{2}\pm(S_{RV}^2+\frac{1}{4}\delta^2)^{\frac{1}{2}}$.

shows $\nu_{obs}-\nu_{calc}$ for the 0,0 violet band; the shifts of the perturbed lines are expressed quantitatively here, and comparison of Fig. 5 with Table II and Fig. 4 shows that the shifts following each perturbed line are in the direction expected. The values of $\nu_{obs}-\nu_{calc}$ plotted in Fig. 5 include the adjustment of Eq. (1) for the value of γ' given later. The amount of the adjustment for each line was calculated as a function of K for that line and a correction made for the resultant shift of the center of each unresolved doublet from the uncorrected calculated positions. The values of ν_{obs} for $K'>15$ are for the components of $K'=J'+\frac{1}{2}$.

It is possible to calculate the value of S_{RV}, the perturbing matrix element, from these measured results. In Fig. 6, R and V are mutually perturbing levels of the same J value, δ is the separation of the corresponding unperturbed levels in cm^{-1}, and Δ is the actual separation (measurable as the difference between the main and the extra line in the λ3883 band). The R and V levels are displaced by equal and opposite amounts from their unperturbed positions. The following equation[21]

$$\Delta=(4S_{RV}^2+\delta^2)^{\frac{1}{2}} \qquad (6)$$

[21] L. N. Liebermann, Phys. Rev. **60**, 504 (1941), Eq. (8).

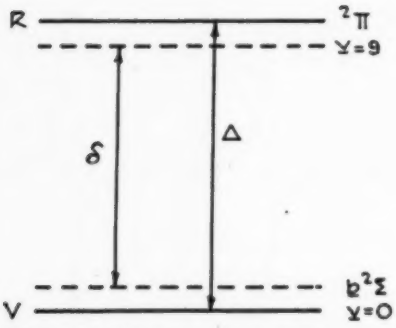

FIG. 6. Schematic diagram of two mutually perturbing levels of the same J value of the red (R) and violet (V) bands of CN. Δ is the actual observed separation of R and V (equal to the separation of a main and corresponding extra line in a violet band) and δ is the corresponding separation of the unperturbed levels in cm^{-1}.

expresses the relation between the known Δ and the unknown S_{RV} and δ.

Since

$$\Delta=\nu(E_V)-\nu(M_V)$$

and

$$\tfrac{1}{2}(\Delta-\delta)=\nu^0(M_V)-\nu(M_V),$$

$(\Delta-\delta)$ and $(\Delta+\delta)$ may be calculated from the observed wave numbers of the perturbed main and extra lines (M and E) of the violet bands, combined with the unperturbed values ν_0 of the main lines taken from a graph or equation for the unperturbed lines. Using the values of Δ given just below Eq. (1) and those of $\frac{1}{2}(\Delta-\delta)$ obtained from Fig. 5, we obtain the following approximate values of S_{RV}^2:

$$S_4^2=0.00758,\quad S_7^2=0.0694,$$
$$S_{11}^2=0.0105,\quad S_{15}^2=0.190.$$

The wave functions of the perturbed levels are

$$\psi_R=(1-\rho^2)^{\frac{1}{2}}\psi_R^0-\rho\psi_V^0,\qquad(7)$$
$$\psi_V=\rho\psi_R^0+(1-\rho^2)^{\frac{1}{2}}\psi_V^0.$$

In the case under consideration, the transitions occur from the upper levels R and V to two lower levels belonging to the $a^2\Sigma$ state, namely, to R'' in $v''=4$ for the red bands and to V'' in $v''=0$ or 1 for the violet CN bands. There will be a "main" line M_R and a weaker "extra" line E_R in the red system bands, and likewise an M_V and an E_V in the violet system bands (see Fig. 7).

Let

$$P_R^0\equiv\left[C\int\psi_R^0P\psi_{R''}^*d\tau\right]^2\equiv a^2,$$
$$P_V^0\equiv\left[C\int\psi_V^0P\psi_{V''}^*d\tau\right]^2\equiv r^2a^2\qquad(8)$$

be the transition probabilities for the unperturbed main lines $R\rightarrow R''$ and $V\rightarrow V''$, respectively. Let it also be supposed that the unperturbed transitions $R\rightarrow V''$ and $V\rightarrow R''$ have negligible intensities. (This seems to be true experimentally.) Then for the actual case

$$M_R:\ P_{RR''}\equiv\left[C\int\psi_RP\psi_{R''}^*d\tau\right]^2=(1-\rho^2)a^2,$$
$$E_R:\ P_{VR''}\equiv\left[C\int\psi_VP\psi_{R''}^*d\tau\right]^2=\rho^2a^2,$$
$$M_V:\ P_{VV''}\equiv\left[C\int\psi_VP\psi_{V''}^*d\tau\right]^2=(1-\rho^2)r^2a^2,\qquad(9)$$
$$E_V:\ P_{RV''}\equiv\left[C\int\psi_RP\psi_{V''}^*d\tau\right]^2=\rho^2r^2a^2.$$

From the theory connecting ρ^2 with S_{RV}^2 and δ^2, one finds [cf. reference 21, Eq. (9)]

$$\rho^2/(1-\rho^2)=(\Delta-\delta)/(\Delta+\delta).\qquad(10)$$

Let the populations of states R and V at any instant be N_R and N_V, respectively. Then, if

$$p\equiv N_R/N_V,\qquad(11)$$

the intensity ratios must be

$$q_V\equiv I(E_V)/I(M_V)=[\rho^2/(1-\rho^2)]N_R/N_V=\left(\frac{\Delta-\delta}{\Delta+\delta}\right)p,$$
$$q_R\equiv I(E_R)/I(M_R)=[\rho^2/(1-\rho^2)]N_V/N_R=\frac{\Delta-\delta}{\Delta+\delta}\left(\frac{1}{p}\right).\qquad(12)$$

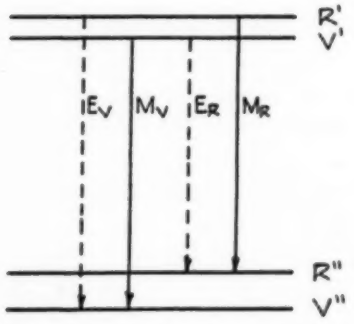

FIG. 7. Schematic diagram showing expected transitions from upper levels R and V to the lower levels R'' in $v''=4$ and V'' in $v''=0$ or 1 for the red and violet CN bands, respectively. The interval $R'-V'$ is actually about three orders of magnitude smaller than $R''-V''$, and its sign in one case is negative. M represents main line and E represents extra line.

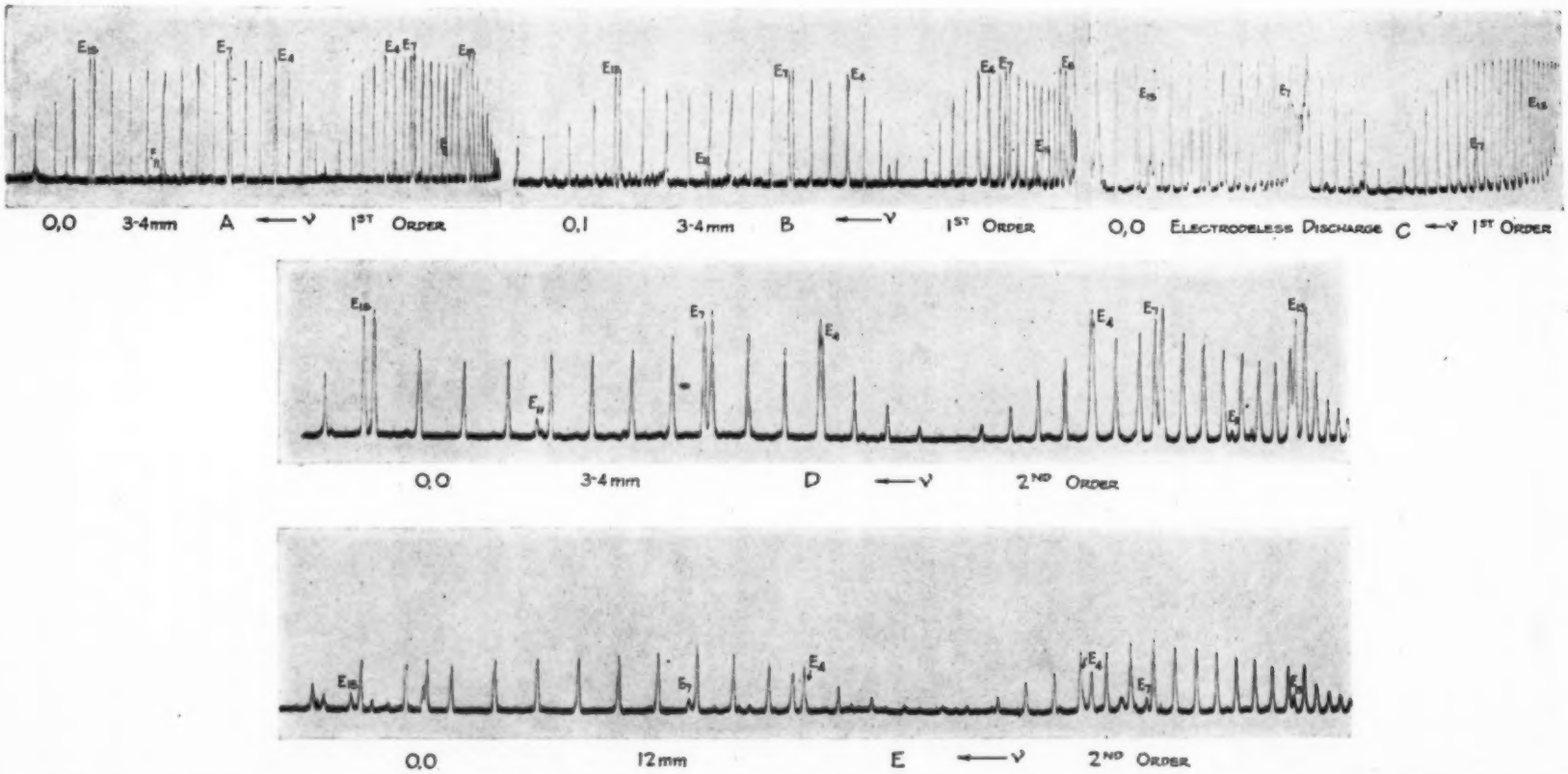

FIG. 8. Microphotometer curves of photographs of violet CN system. *R* branch on left in all traces, *P* branch on right. $E_{K'}$ denotes extra lines. The perturbed and extra lines are noticeably enhanced except in traces *C* and *E*. Traces *A*, *B*, and *D* are made from plates obtained by mixing $CHCl_3$ with active nitrogen—photographs all made during same exposure. Trace *E* is from same source operated at higher pressure. Trace *C* (reference 22) is from plate obtained with stopcock grease as small impurity in electrodeless discharge. Traces *C* and *E* show less enhancement of perturbed and extra lines and fewer extra lines.

TABLE IV. Values of $\frac{\Delta-\delta}{\Delta+\delta}$, q_v, $p_{K'}$, ρ^2, and $(1-\rho^2)$ obtained from the 0,0 violet band.

K'	$\Delta-\delta/\Delta+\delta$	q_v	$p_{K'}$	q_R	ρ^2	$1-\rho^2$
4	0.0699	1	14	0.005	0.065	0.935
7	0.0945	1	10	0.0095	0.086	0.914
11	0.0077	1/6	22	0.00035	0.00764	0.99236
15	0.179	1	6	0.0298	0.152	0.848

The microphotometer traces, Fig. 8, give a qualitative measure of q_v. Trace A, λ3883 in first order, and trace B, λ4216 in first order, show that $q_v \sim 1$ for the perturbations at $K'=4$, 7, and 15 at a pressure of 3–4 mm and $q_v \ll 1$ for the perturbation at $K'=11$. Trace C, taken from a plate made by Dr. S. Mrozowski[22] under radically different discharge conditions (electrodeless discharge in a heated tube containing bismuth vapor at perhaps a few tenths mm pressure, helium at 1- or 2-mm pressure, and a trace of stopcock grease), shows only the extra lines at $K'=7$ and 15, respectively, in λ3883, both with $q_v \ll 1$. Trace D is from the same exposure as Trace A (λ3883 at 3–4 mm), but in second order. Trace E shows λ3883 in second order at 12 mm. At this pressure, the extra lines at $K'=7$ and 15, respectively, are the only ones which appear, and the enhancements are very small. Also, $q_v \ll 1$ in this case. These relations resemble those on Dr. Mrozowski's plate. Reasons for the variations of q_v, and therefore p, with pressure will be discussed later.

A study of the microphotometer traces shows that $q_v \sim 1$ for $K'=4$, 7, and 15, and $q_v \sim 1/6$ for $K'=11$ at 3–4 mm. Equation (12) states that

$$q_v = \left(\frac{\Delta-\delta}{\Delta+\delta}\right) p.$$

Substitution of the values of Δ and δ used in the calculation of S_{RV}^2 yields experimental values of $p \equiv N_R/N_V$, for the photographs at 3–4-mm pressure (see Table IV). If now these values of p are substituted in the second of Eq. (12), values for q_R can be predicted, and are all found to be 0.03 or less. Thus, on this basis, the experimentally observed absence of extra lines in the red 9,4 band as photographed at 3–4-mm pressure seems to be very satisfactorily explained. At 12-mm pressure, where the photographs of λ3883 indicate that $p=1$ may be approached, one can now predict that the extra lines in the red bands might be visible, but unfortunately no suitable plates of the red bands were obtained under these conditions.

Substitution of the values of ρ^2 and $(1-\rho^2)$ from columns 6 and 7, respectively, in Table IV yields the following transition probabilities as given in Table V. The quantities a^2 and r^2 should be substantially the same for all K values.

Now let N_V^0 be the population of an unperturbed level (N_V^0 is, of course, a function of K); then one may define

$$m \equiv N_V/N_V^0 \tag{13}$$

for any perturbed V level. One may determine m approximately by drawing a smooth curve through the least perturbed violet band line intensities to estimate an N_V^0 for the given perturbed line. Such an estimate obtained with the aid of a microphotometer trace of a band taken at a pressure of 3–4 mm yields: $m_4 \sim 1.2$, $m_7 \sim 1.1$, $m_{11} \sim 1.0$, and $m_{15} \sim 1.25$. In the band obtained by S. Mrozowski (see Fig. 8), it may be observed that $m \sim 1.0$ for the two perturbations observed there.

This phenomenon of enhancement of the perturbed main lines and the extra lines in the violet band, and the lack of enhancement or weakening of the perturbed main lines and the absence of the extra lines in the associated red band, requires that a collision process be postulated. The process must be one in which rapid $R \rightarrow V$ transfer occurs at the K values where there are perturbations. Further, it must be such that the perturbed rotational levels of the red band are repopulated by rotational redistribution collisions at about the same rate as they are depopulated by collision transfer to the perturbed

TABLE V. Transition probabilities.

K'	$P_{RR''}$	$P_{VR''}$	$P_{VV''}$	$P_{RV''}$
4	$0.935a^2$	$0.065a^2$	$0.935r^2a^2$	$0.065r^2a^2$
7	$0.914a^2$	$0.086a^2$	$0.914r^2a^2$	$0.086r^2a^2$
11	$0.99236a^2$	$0.00764a^2$	$0.99236r^2a^2$	$0.00764r^2a^2$
15	$0.848a^2$	$0.152a^2$	$0.848r^2a^2$	$0.152r^2a^2$

[22] The author wishes to thank Dr. Mrozowski for his kindness in permitting him to use the plate from which this trace was made.

violet levels and emission in the violet band. This is in agreement with the prediction of Beutler and Fred (cf. reference 3), where the effect of pressure is discussed. The effect would be "smoothed out" at very high or very low pressures. The traces in Fig. 8 obtained from plates (with the exception of S. Mrozowski's) made at medium pressures, indicate that apparently there is such an effect. The "smoothing out" in S. Mrozowski's plate may be caused by a higher temperature in the discharge tube (experimentally true) or by very low partial pressure of the CN present.

It is probable that the colliding molecules which are effective in repopulating the depleted rotational levels are CN molecules. It would be necessary to perform a new set of experiments ranging down to 0.5-mm pressure in order to check completely the effect of pressure; it might even be advisable to use different admixed substances and different temperatures of the mixing tube. The discharge system used here is not suitable for such low pressures because the stray discharge becomes too intense at these pressures.

During the discussion of the 0,0 violet band, it was stated that the doubling in the $^2\Sigma$ state becomes noticeable at $K'=16$. The doublets were observed to have one strong component and one very weak component (see Fig. 9), the strong component being on the higher wave number side. The intensity of this component falls off rapidly, with increasing K, and appears visually to have nearly the same intensity as the weak component at higher K ($K'=20$, 21, and 22). The doublet splitting was measured, and the value of $(\gamma'-\gamma'')$ determined to be $+0.0110$. Birge[23] gives $(\gamma'-\gamma'')=0.0090$ from CN bands obtained with a hot source. Comparison of $(\gamma'-\gamma'')=+0.0110$ with $\gamma''=+0.0104$ obtained by extrapolation from the results of Jenkins, Roots, and Mulliken[24] gives $\gamma'=+0.0214$.

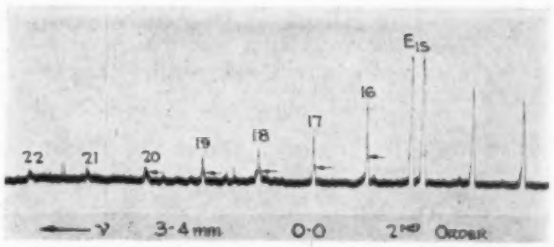

FIG. 9. Microphotometer curve of R branch of 0,0 violet band for larger values of K'. The strong doublet components with $J'=K'+\frac{1}{2}$ and the weak components with $J'=K'-\frac{1}{2}$ appear for $K'\geq 16$; for $K'\geq 20$, both components are weak and of comparable intensity.

The intensification of one series of doublet components may be explained according to the following interesting mechanism. They have $J'=K'+\frac{1}{2}$ like the perturbed line $K'=15$, and are intense because of collision enhancement either directly like the perturbed line, or indirectly as a result of collision enhancement of $J'=15\frac{1}{2}$ followed by collisions which change K' by one or a few units without changing the direction of the spin. The weak doublet components then have $J'=K'-\frac{1}{2}$; their intensity may be near the natural intensity without collision enhancement, or they may also have been enhanced somewhat by collisions, but much less than for $J'=K'+\frac{1}{2}$ because the perturbed lines which have $J'=K'-\frac{1}{2}$ are weak or remote from the $K'=15$ region.

The author wishes to express his appreciation of invaluable advice and criticism of the late Dr. H. G. Beutler and of Professor R. S. Mulliken in the solution of the experimental and theoretical problems involved.

[23] R. T. Birge, Astrophys. J. **55**, 280 (1922).

[24] See reference 16, pp. 29–30.

The Effect of Pressure upon the Dielectric Constants of Liquids

BENTON BROOKS OWEN, *Sterling Chemistry Laboratory, Yale University, New Haven, Connecticut*

AND

STUART R. BRINKLEY, JR.,* *Mallinckrodt Chemical Laboratory, Harvard University, Cambridge, Massachusetts***

(Received May 18, 1943)

An empirical equation containing two parameters A and B is shown to express the isothermal variation of the dielectric constants of liquids with pressure. The equation is analogous to the Tait equation for the variation of the densities of liquids with pressure. The parameter B is common to both equations, and therefore may be determined independently from either dielectric constants or densities. Furthermore B can be eliminated between the two equations to give a linear relationship between the reciprocals of the dielectric constant and the density. It is shown that this linear relationship may be derived from Tammann's hypothesis and electrostatic theory.

(1) INTRODUCTION

An accurate knowledge of the pressure dependence of the dielectric constants (D) of various solvents is of great importance in the study of certain partial molal properties of electrolytes in solution.[1] Good values of D and $\partial(1/D)/\partial P$ will suffice for the study of partial molal volumes, but $\partial^2(1/D)/\partial P^2$ and $\partial^2(1/D)/\partial P\partial T$ are required for partial molal compressibilities and expansibilities. Since dielectric constant measurements at high pressures are usually less precise than those at one atmosphere, the second derivatives cannot be satisfactorily evaluated unless the proper functional relationship between D and P is known. It is our purpose to show that this relationship takes the simple form[2]

$$1-\frac{D^{(1)}}{D^{(P)}}=AD^{(1)}\log\frac{B+P}{B+1} \tag{1}$$

for pressures up to several thousand atmospheres and appears to be completely analogous to the Tait[3] equation

$$1-\frac{\rho^{(1)}}{\rho^{(P)}}=C\rho^{(1)}\log\frac{B+P}{B+1} \tag{2}$$

written in terms of the density, ρ.

The parameters of these equations, A, B, and C, are independent of the pressure. B is a function of the temperature, usually decreasing with increasing T. Gibson[4] has shown that Eq. (2) accurately represents the available data up to 10,000 atmospheres and that the product $C\rho^{(1)}$ is independent of the temperature. The results given in the next section indicate that $AD^{(1)}$ is also independent of T, but the evidence is not conclusive. If further measurements verify the temperature independence of $AD^{(1)}$, the analogy between Eqs. (1) and (2) would be complete. This point has practical as well as theoretical interest, for if A can be evaluated at any one temperature from dielectric constants under pressure, the derivatives

$$\left(\frac{\partial(1/D)}{\partial P}\right)^{(P)}=-\frac{0.4343A}{B+P}, \tag{3}$$

$$\left(\frac{\partial^2(1/D)}{\partial P^2}\right)^{(P)}=\frac{0.4343A}{(B+P)^2}, \tag{4}$$

$$\left(\frac{\partial^2(1/D)}{\partial P\partial T}\right)^{(P)}=\frac{0.4343A}{(B+P)^2}\left(\frac{\partial B}{\partial T}\right)+\frac{0.4343A}{D^{(1)}(B+P)}\left(\frac{\partial D}{\partial T}\right)^{(1)} \tag{5}$$

could be evaluated at any temperature at which $D^{(1)}$ and B are known as functions of T. The fact that B can be conveniently determined from

* National Research Fellow in Chemistry.

** Present address, Department of Chemistry, Cornell University, Ithaca, New York.

[1] F. T. Gucker, Jr., Chem. Rev. **13**, 111 (1933).

[2] The pressure at which a quantity is measured is indicated in parenthesis as a superscript.

[3] P. G. Tait, "Report on some of the physical properties of fresh water and sea water," *Physics and Chemistry of the Voyage of H.M.S. Challenger*, Vol. II, Part IV, S.P., LXI (1888).

[4] R. E. Gibson, J. Am. Chem. Soc. **56**, 4 (1934); *ibid.*, **57**, 284 (1935). See also A. Wohl, Zeits. f. physik. Chemie **99**, 234 (1921), and H. Carl, *ibid.* **101**, 238 (1922).

TABLE I. Comparison of Eq. (1) with experimental data.

Liquid	$t°$	#	P_{max}	$D^{(1)}$	$AD^{(1)}$	B^a	Δ_{Av}	Δ_{max}
				Data of Kyropoulos				
Water	20	7	3000	80.79	0.4060	2963*	0.06	0.15
Methanol	20	7	3000	33.79	.2905	1187	.07	.16
Ethanol	20	7	3000	25.71	.2663	1255	.08	.23
Acetone	20	7	3000	21.50	.2577	784	.08	.19
Pyridine	15	11	2500	13.93	.3504	1667	.05	.18
Chloroform	18.5	7	3000	4.955	.2478	916	.05	.23
Ethyl ether	20	7	3000	4.328	.3707	588	.09	.17
Carbon disulfide	20	7	3000	2.647	.2516	1275	.12	.26
Benzene	18	3	400	2.288	.1327[b]	1021*	.10	.30
Carbon tetrachloride	18	5	1000	2.246	.1581[b]	916*	.23	.55
Petroleum ether	18.4	7	3000	1.870	.1398	588	.06	.10
				Data of Danforth				
Glycerol	0	7	8000	49.9	0.3708	3838	0.08	0.16
Glycerol	30	8	12000	42.8	.4032	3664	.11	.28
Ethanol	0	8	12000	(27.7)	.3030	1884	.19	.54
Ethanol	30	8	12000	(23.3)	.3048	1290	.34	.83
i-Butanol	0	8	12000	(21.7)	.2469	1623	.48	2.75
i-Butanol	30	8	12000	17.3	.2521	1034	.19	.36
Hexanol	30	5	4000	12.90	.4210	3391	.04	.08
Hexanol	75	7	8000	8.55	.2197	742	.25	.63
Eugenol	30	5	3000	10.49	.2544	1967	.39	.84
Chlorobenzene	30	5	4000	5.41	.2240	1210*	.10	.28
Chlorobenzene	75	7	8000	4.90	.2219	897*	.15	.34
Bromobenzene	30	5	4000	5.22	.1880	1364*	.02	.04
Bromobenzene	75	7	8000	4.87	.1923	1036*	.12	.26
Ethyl ether	30	8	12000	4.15	.3506	608	.50	.93
Ethyl ether	75	7	12000	(3.39)	.3612	507	.64	1.67
Carbon disulfide	30	8	12000	(2.63)	.2203	1013	.20	.85
Carbon disulfide	75	6	12000[c]	(2.47)	.2428	871	.05	.29
Pentane	30	8	12000	1.82	.1729	709	.06	.53
Pentane	75	6	12000[c]	(1.78)	.1726	608	.08	.47
				Data of Francke				
Benzene	18	14	700[d]	(2.2709)	0.1327	1021*	0.03	0.07
Carbon tetrachloride	18	16	800[d]	(2.2220)	.1581	916*	.02	.04
Heptane	18	16	800[d]	(1.9400)	.1118	608	.02	.06
Hexane	18	16	800[d]	(1.8220)	.1299	658	.02	.05

Values in parenthesis extrapolated from results at higher pressures.
Number of pressures at which D was measured.
P_{max} Upper limit of experimental pressure range. Lower limit 1 atmos. unless otherwise noted.
Δ_{Av} and Δ_{max} percent difference between $D^{(P)}$ observed and calculated by Eq. (1).
* Values of B derived from compressibility data of Gibson.
[a] All values of B have been converted to bars for consistency in tabulation, although some of the data were expressed in atmospheres and some in kg per cm².
[b] From Francke's data below.
[c] Lower pressure limit 1000 atmos.
[d] Lower pressure limit 50 atmos.

density (compressibility) data extends the range of such calculations enormously, for very little work has been done on dielectric constants under pressure at more than one temperature.

Another important feature of Eqs. (1) and (2) is that elimination of the common term yields the linear relationship

$$1-\frac{D^{(1)}}{D^{(P)}}=\frac{AD^{(1)}}{C\rho^{(1)}}\left(1-\frac{\rho^{(1)}}{\rho^{(P)}}\right) \qquad (6)$$

between the reciprocals of the dielectric constant and the density. In Section (3) it will be shown that this simple relationship can be derived from Tammann's hypothesis and electrostatic theory. The analogy between the two empirical Eqs. (1) and (2) is therefore not fortuitous because either one may be derived from the other with the aid of Eq. (6).

(2) VERIFICATION OF THE EQUATIONS BY COMPARISON WITH EXPERIMENTAL RESULTS

Table I contains the results of fitting Eq. (1) to the experimental data of Kyropoulos,[5] Danforth,[6] and Francke.[7] The parameters were

[5] S. Kyropoulos, Zeits. f. Physik **40**, 507 (1926).
[6] W. E. Danforth, Jr., Phys. Rev. **38**, 1224 (1931).
[7] C. Francke, Ann. d. Physik **77**, 159 (1925).

TABLE II. Re-evaluation of the parameters of Eq. (1) keeping $AD^{(1)}$ independent of the temperature.

Liquid	$t°$	$D^{(1)}$	$AD^{(1)}$	B	Δ_{Av}	Δ_{max}	Data
Glycerol	0	49.9	0.3870	4090	0.07	0.21	Danforth
Glycerol	30	42.8	.3870	3424	.14	.32	Danforth
Ethanol	0	(27.7)	.3039	1884	.32	.62	Danforth
Ethanol	20	25.71	.3039	1452	.24	.88	Kyropoulos
Ethanol	30	(23.3)	.3039	1290	.36	.79	Danforth
i-Butanol	0	(21.7)	.2495	1644	.49	2.75	Danforth
i-Butanol	30	17.3	.2495	1023	.18	.53	Danforth
Hexanol	30	12.90	.2200[a]	1309	.54	1.06	Danforth
Hexanol	75	8.55	.2200[a]	752	.25	.63	Danforth
Chlorobenzene	30	5.41	.2230	1210*	.11	.35	Danforth
Chlorobenzene	75	4.90	.2230	897*	.15	.40	Danforth
Bromobenzene	30	5.22	.1902	1364*	.06	.19	Danforth
Bromobenzene	75	4.87	.1902	1036*	.17	.33	Danforth
Ethyl ether	20	4.328	.3559	541	.07	.31	Kyropoulos
Ethyl ether	30	4.15	.3559	630	.55	1.11	Danforth
Ethyl ether	75	(3.39)	.3559	497	.71	2.30	Danforth
Carbon disulfide	20	2.647	.2316	1133	.16	.30	Kyropoulos
Carbon disulfide	30	(2.63)	.2316	1100	.30	.77	Danforth
Carbon disulfide	75	(2.47)	.2316	776	.20	.26	Danforth
Petane	30	1.82	.1728	709	.06	.53	Danforth
Petane	75	1.78	.1728	608	.08	.47	Danforth

* Values of B derived from compressibility data of Gibson.
[a] In this case the average value of $AD^{(1)}$ was not used. The value at 75° was chosen as being more in line with the general trend for the alcohols. This choice gives a more "reasonable" value of B at 30°, but increases the deviations considerably.

evaluated by the method of least squares. In this procedure, infinite weight was given to the value of $D^{(1)}$ except for those liquids for which $D^{(1)}$ was not recorded,[8] or was clearly inconsistent with the results at higher pressures.[9] In these exceptional cases $D^{(1)}$ was treated as a third empirical parameter and evaluated accordingly. Whenever B could be obtained from Gibson's[10] compressibility data, this value was used, and only A had to be evaluated from the measurements of $D^{(P)}$. This simultaneous use of Eqs. (1) and (2) is equivalent to the use of Eq. (6), so no separate verification of the latter equation will be given.[11]

The average and maximum differences (percent) between observed values of $D^{(P)}$ and those calculated by Eq. (1) are given in the last two columns of Table I. With only two exceptions,[12] these differences show that the equation will represent the data to within a few units in the last significant figure in $D^{(P)}$. This is very good agreement indeed, considering the wide range in D and P covered by the experiments and the fact that in one-third of the comparisons B was calculated from compressibility data. Furthermore, in comparing the equation with Kyropoulos' data for benzene and carbon tetrachloride, both A and B were derived from other sources.

Table I also shows that the values of $AD^{(1)}$ obtained from Danforth's data are insensitive to the temperature, particularly if an accurate value of B from compressibilities is employed. In order to investigate this point, we have averaged the values of $AD^{(1)}$ from Danforth's data in Table I and re-evaluated B. The results are given in Table II, where it can be seen that the assumption of the temperature independence of $AD^{(1)}$ has very little effect upon the concordance between Eq. (1) and experiment. The means of the values of Δ_{Av} and Δ_{max} in Table II are 0.24 and 0.72, while the means of the corresponding values in Table I are only slightly less, *viz.*, 0.20 and 0.58. Only in the case of ethanol at 20° were eight experimental points on the curve for *i*-butanol at 0° is quite out of line, and if this point is neglected the differences are reduced to 0.15 and 0.25. Ethyl ether at 75° might easily yield erroneous results if contaminated by certain impurities.

[8] Danforth's data for carbon disulfide (75°), pentane (75°), and the data of Francke.
[9] Danforth's ethanol (0 and 30°), *i*-butanol (0°), ethyl ether (75°), and carbon disulfide (30°).
[10] Values of B for a number of solvents at 25 to 85° were kindly supplied by Dr. R. E. Gibson of the Geophysical Laboratory, Washington, D. C. For purposes of interpolation and extrapolation, we fitted these values to cubic equations in (t-25) by the method of least squares.
[11] The values of $D^{(P)}$ and $\rho^{(P)}$ recorded by Danforth are unsuitable for a direct test of Eq. (6) because the data are not given to a sufficient number of significant figures, and are not always consistent with the accepted values of $D^{(1)}$ and $\rho^{(1)}$.
[12] It is not unreasonable to attribute these unusually large differences to experimental errors. Thus, one of the

systematic departures from the equation caused by keeping $AD^{(1)}$ independent of temperature.

There is one other verification of Eq. (1) which is worthy of note. Since the dielectric constant of a liquid of unit permeability is equal to the square of the index of refractions, we can write Eq. (1) in the form

$$1-\frac{n^{2(1)}}{n^{2(P)}}=An^{2(1)}\log\frac{B+P}{B+1} \qquad (7)$$

for such liquids. Table III shows the results of fitting this equation to the data of Gibson and Kincaid[13] for benzene, a liquid for which the permeability is very close to unity. The ability of the equation to represent the data with high precision is remarkable, particularly because B was determined from compressibilities, and only the one parameter, A, was adjusted to fit the index of refraction data. This constitutes a very good indication of the validity of Eq. (6). Furthermore, $An^{2(1)}$ is practically independent of the temperature and may be made absolutely independent of T without seriously increasing the differences between the equation and experiment.

(3) THEORETICAL

The derivation of Eq. (6) involves the calculation of the electrostatic contribution, $V_e^{(P)}$, to the partial molal volume of an electrolyte at infinite dilution by two independent methods. In both calculations $V_e^{(P)}$ is necessarily a function of the radii and other characteristics of the individual ions, but $\partial \log V_e^{(P)}/\partial P$ can be made independent of these characteristics if they are properly chosen. Equation (6) then follows by equating the two expressions for $\partial \log V_e^{(P)}/\partial P$. Since the resulting equation involves only properties of the pure solvent (D and ρ), it should be independent of the characteristics of the ions which were arbitrarily introduced in its derivation. If this be true, the validity of our derivation of the equation depends primarily upon the possibility of endowing a hypothetical electrolyte with properties which simultaneously fulfill all the conditions subsumed in the two independent calculations of $\partial \log V_e^{(P)}/\partial P$.

With these conditions in mind, we will consider a hypothetical electrolyte which dissociates completely into two spherical ions of equal radii (b) supporting equal charges ($\pm z\epsilon$) uniformly distributed upon their surfaces. The ions are incompressible, are very large compared to the solvent molecules, and would behave as ideal solutes in the absence of their charges.

According to Tammann[14] the contraction in volume and decrease in compressibility which accompanies the addition of an electrolyte to a solvent can be ascribed to a compression of the solvent, rather than to any alteration in the solute (other than melting). The pressure increment, P_e, which would be required to produce this compression of the solvent is called the "effective pressure." P_e is a function of the concentration and the properties of the ions and the solvent, but is assumed independent of the external pressure, P, upon the solution. The effective pressure has been very useful in interpreting the behavior of electrolytic solutions, and Gibson[4] has shown that its introduction into the Tait Eq. (2) permits a quantitative representation of the densities and compressibilities of such solutions within the experimental errors.

Since Tammann's hypothesis represents the behavior of real ionic solutions to a close approximation, it should very satisfactorily describe a solution containing our hypothetical incompressible ions. Accordingly we write

$$V^{(P)}=mV_2+1000v^{(P+P_e)} \qquad (8)$$

for the total volume of the solution in terms of the ideal molal volume of the solute, V_2; and the specific volume of the pure solvent, v. Note that

TABLE III. Comparison of Eq. (7) with experimental data for the index of refraction of benzene

λ^a	t°	#	P_{max}	$n^{(1)}$	$An^{2(1)}$	B	Δ_{Av}	Δ_{max}
589	25	4	868	1.4983	0.1569	970*	0.008	0.019
589	35	4	1030	1.4918	.1564	899*	.014	.026
589	45	4	1188	1.4851	.1562	829*	.016	.029
436	25	4	561	1.5201	.1608	970*	.006	.016
436	35	4	713	1.5134	.1587	899*	.011	.021
436	45	4	867	1.5065	.1582	829*	.008	.020

* Values of B derived from compressibility data of Gibson.
[a] Wave-length of the light used (mμ).

[13] R. E. Gibson and J. F. Kincaid, J. Am. Chem. Soc. **60**, 511 (1938).

[14] G. Tammann, *Über die Beziehungen zwischen den innern Kräften und Eigenschaften der Lösungen* (Voss, Liepzig, 1907), p. 36.

the apparent volume of the solvent in the solution under the pressure P is represented by the volume of the same quantity of pure solvent under a pressure $P+P_e$. In dilute solutions of large ions, P_e is small, and Eq. (8) may be written

$$V^{(P)}-mV_2=1000v^{(P)}+1000(\partial v/\partial P)^{(P)}P_e \quad (9)$$

and, since the partial molal volume, $\bar{V}_2$, is defined as $(\partial V/\partial m)_{T,P}$, we obtain

$$\bar{V}_2{}^{(P)}-V_2=1000(\partial v/\partial P)^{(P)}(\partial P_e/\partial m). \quad (10)$$

At infinite dilution the left-hand member of this equation is $\bar{V}^\circ{}_2{}^{(P)}-V_2$. The term $\bar{V}^\circ{}_2{}^{(P)}$ includes the effect of electrostriction of the solvent, and V_2 is the ideal molal volume of the ions in the absence of electrostriction. The difference between these two volumes is therefore the quantity V_e. Consequently

$$V_e^{(P)}=\bar{V}^\circ{}_2{}^{(P)}-V_2$$

$$=1000(\partial v/\partial P)^{(P)}(\partial P_e/\partial m)_{m=0} \quad (11)$$

and

$$\frac{\partial \log V_e^{(P)}}{\partial P}=(\partial^2 v/\partial P^2)^{(P)}/(\partial v/\partial P)^{(P)} \quad (12)$$

is the result obtained from Tammann's hypothesis.

From consideration of the reversible electrical work (per mole) of charging the ions of an electrolyte at infinite dilution, the electrostatic contribution to the partial molal free energy[15] of the electrolyte is found to be

$$\bar{F}^\circ{}_2-F_2=z^2\epsilon^2N/bD^{(P)}, \quad (13)$$

when the cations and anions have equal radii and charges. Although the electrical work is most simply calculated[16] by assuming that the ions are uniformly charged spheres in a homogeneous medium of dielectric constant D, alternative calculations[17] which consider the inhomogeneity of the solvent lead to essentially the same result for very large ions. The properties assigned to our hypothetical electrolyte not only fulfill the conditions underlying Eq. (13), but also require the derivative* of this expression to take the simple form

$$V_e^{(P)}=\bar{V}^\circ{}_2{}^{(P)}-V_2=\left(\frac{z^2\epsilon^2N}{b}\right)\left(\frac{\partial(1/D)}{\partial P}\right)^{(P)}, \quad (14)$$

because the radii of incompressible ions are independent of the pressure.

Logarithmic differentiation of Eq. (14) yields

$$\left(\frac{\partial \log V_e}{\partial P}\right)^{(P)}=\left(\frac{\partial^2(1/D)}{\partial P^2}\right)^{(P)}\Big/\left(\frac{\partial(1/D)}{\partial P}\right)^{(P)} \quad (15)$$

for the electrostatic calculation of the same quantity given by Eq. (12), from Tammann's hypothesis. Combination of Eqs. (12) and (15) gives the differential equation

$$\left(\frac{\partial^2(1/D)}{\partial P^2}\right)^{(P)}\Big/\left(\frac{\partial(1/D)}{\partial P}\right)^{(P)}$$

$$=\left(\frac{\partial^2 v}{\partial P^2}\right)^{(P)}\Big/\left(\frac{\partial v}{\partial P}\right)^{(P)} \quad (16)$$

from which Eq. (6) is obtained by integration.

[15] G. Scatchard, Chem. Rev. **3**, 383 (1927); J. Chem. Phys. **9**, 34 (1941).

[16] M. Born, Zeits. f. Physik **1**, 45 (1920); E. Guntelberg, Zeits. f. physik. Chemie **123**, 199 (1926).

[17] P. Debye and J. McAulay, Physik. Zeits. **26**, 22 (1925); P. Debye, Zeits. f. physik. Chemie **130**, 56 (1927); J. A. V. Butler, J. Phys. Chem. **33**, 1015 (1929); H. S. Harned and N. N. T. Samaras, J. Am. Chem. Soc. **54**, 9 (1932).

* $(\partial F/\partial P)_T=V$.

A Note on the Thermoelectromotive Force*

KARL F. HERZFELD
Catholic University of America, Washington, D. C.
(Received May 10, 1943)

A simple kinetic interpretation of the thermoelectromotive force, applicable in quantum theory and classical theory, is given. It is shown that the usual expression can be transformed so as to agree with our result.

IT is possible to give simple physical interpretations for many formulae in the electron theory of metals and semi-conductors, but that has not been done for the thermoelectromotive force. The present attempt is based on a remark of Einstein,[1] comparing the state of electrons in a temperature gradient to that of a gas at low pressure in a capillary in which a temperature gradient exists. Because collisions occur only with the walls, not between gas molecules, the molecules *leaving* a spot on the wall have equilibrium distribution.

Call dz the number of states having energies between ϵ and $\epsilon+d\epsilon$ and assume that the distribution of directions in space is isotropic. Then the number of electrons moving with energy between ϵ and $\epsilon+d\epsilon$ within the solid angle $d\Omega$ is given in equilibrium by

$$dn=fdz(d\Omega/4\pi).$$

We assume that at the last collision, "which occurred at a distance l (mean free path)," the electrons take on the equilibrium distribution at the corresponding place.

If there is a temperature gradient in the x direction, the simplest consideration gives as the excess flow per second through a unit area located at x, of those electrons which have an energy between ϵ and $\epsilon+d\epsilon$

$$dz\tfrac{1}{4}\bar{v}\{f(x-l)-f(x+l)\}=-dz\tfrac{1}{4}\bar{v}2l(\partial f/\partial x), \quad (1)$$

$x-l$, $x+l$ being the argument of f, and $\bar{v}$ the average velocity belonging to ϵ.

A more exact calculation considers that a molecule, the motion of which makes an angle θ with the x axis and which comes from the distance l, travels $l\cos\theta$ in the x direction.

Therefore, the resultant flow in the x direction is

$$dz\int_0^\pi \bar{v}\cos\theta f(x-l\cos\theta)\sin\theta d\theta(2\pi/4\pi)$$
$$=-dz\bar{v}l(\partial f/\partial x)\tfrac{1}{2}\int_0^\pi \cos^2\theta\sin\theta d\theta$$
$$=-\tfrac{1}{3}\bar{v}l(\partial f/\partial x)dz. \quad (2)$$

In the first part of (2), $x-l\cos\theta$ is the argument of f. The total current is

$$I_x'=-\tfrac{1}{3}e\int l\bar{v}(\partial f/\partial x)dz$$
$$=-(\partial T/\partial x)\tfrac{1}{3}e\int l\bar{v}(\partial f/\partial T)dz. \quad (3)$$

To keep the system without current, we must have an electric field F, given by

$$\sigma F-(\partial T/\partial x)\tfrac{1}{3}e\int l\bar{v}(\partial f/\partial T)dz=0, \quad (4)$$

where σ is the conductivity.

The differential thermoelectromotive force Θ defined as

$$\Theta=-\lim_{\Delta T=0}\frac{\oint Fdx}{\Delta T}$$

is then

$$\Theta=+\left[\frac{e}{3\sigma}\int l\bar{v}\frac{\partial f}{\partial T}dz\right]_1-\left[\frac{e}{3\sigma}\int l\bar{v}\frac{\partial f}{\partial T}dz\right]_2, \quad (5)$$

the indices 1 and 2 referring to the two substances. If both electrons and holes are present, (4) is replaced by

$$F=-\frac{\partial V}{\partial x}=\frac{1}{\sigma_++\sigma_-}\frac{|e|}{3}\int\left\{\bar{v}_+l_+\left(\frac{\partial f}{\partial T}\right)_+\left(\frac{dz}{d\epsilon}\right)_+\right.$$
$$\left.-\bar{v}_-l_-\left(\frac{\partial f}{\partial T}\right)_-\left(\frac{dz}{d\epsilon}\right)_-\right\}d\epsilon. \quad (4')$$

* This paper originated from a suggestion by Dr. Lark-Horovitz.

[1] See K. F. Herzfeld, Ann. d. Physik **41**, 43 (1913).

If l is independent of the temperature (but still possibly dependent on ϵ) (4) can be written

$$F=-\frac{1}{\sigma}\frac{\partial}{\partial T}\frac{e}{3}\int l\bar{v}f dz. \qquad (4'')$$

We want to show that (4) is identical with the exact formula. The latter can be written[2]

$$I=-\frac{e}{3}\left[\left\{e(-F)+kT\left(\frac{\partial}{\partial x}\frac{\zeta}{kT}\right)\right\}\right.$$
$$\left.\times\int_0^\infty l\bar{v}\left(-\frac{\partial f}{\partial \epsilon}\right)dz+\frac{1}{T}\frac{\partial T}{\partial x}\int_0^\infty l\bar{v}\epsilon\left(-\frac{\partial f}{\partial \epsilon}\right)dz\right]. \qquad (6)$$

The notation has been changed and generalized. We have written vdz for Fowler's $(8\pi\tilde{\omega}m/h^3)\epsilon d\epsilon$ and (ζ/kT) for $\ln\lambda$. ζ is the chemical potential per electron.

We transform now (6) by writing

$$\frac{\partial}{\partial x}\frac{\zeta}{kT}=\left(\frac{\partial}{\partial x}\frac{\zeta}{kT}\right)_T+\frac{\partial T}{\partial x}\frac{\partial}{\partial T}\frac{\zeta}{kT}$$

and

$$F=-\frac{\partial V}{\partial x}.$$

$$kT\left(\frac{\partial}{\partial x}\frac{\zeta}{kT}\right)_T=\left(\frac{\partial}{\partial x}\zeta\right)_T$$

is the change of the chemical potential because of the change in material. Then

$$I=-\frac{\sigma}{e}\left[+e\frac{\partial V}{\partial x}+\left(\frac{\partial \zeta}{\partial x}\right)_T\right]$$
$$-\frac{e}{3}\frac{\partial T}{\partial x}\int_0^\infty\left[kT\frac{\partial}{\partial T}\frac{\zeta}{kT}+\frac{\epsilon}{T}\right]l\bar{v}\left(-\frac{\partial f_0}{\partial \epsilon}\right)dz. \qquad (7)$$

f can be written for all three statistics as

$$f=[e^{(\epsilon-\zeta)/kT}+\gamma]^{-1}, \qquad (8)$$

γ being $+1$ (Fermi-Dirac), -1 (Einstein-Bose) or 0 (Boltzmann). From (8)

$$\frac{\partial f}{\partial T}=\frac{e^{(\epsilon-\zeta)/kT}}{(e^{(\epsilon-\zeta)/kT}+\gamma)^2}\frac{\partial}{\partial T}\left(\frac{\zeta-\epsilon}{kT}\right)$$
$$=\frac{e^{(\epsilon-\zeta)/kT}}{(e^{(\epsilon-\zeta)/kT}+\gamma)^2}\left[\frac{\partial}{\partial T}\frac{\zeta}{kT}+\frac{\epsilon}{kT^2}\right]$$
$$=-kT\frac{\partial f}{\partial \epsilon}\left[\frac{\partial}{\partial T}\frac{\zeta}{kT}+\frac{\epsilon}{kT^2}\right]$$
$$=-\frac{\partial f}{\partial \epsilon}\left[kT\frac{\partial}{\partial T}\frac{\zeta}{kT}+\frac{\epsilon}{T}\right].$$

Therefore (7) can be rewritten

$$I=-\frac{\sigma}{e}\left[+e\frac{\partial V}{\partial x}+\left(\frac{\partial \zeta}{\partial x}\right)_T\right]-\frac{e}{3}\frac{\partial T}{\partial x}\int_0^\infty lv\frac{\partial f}{\partial T}dz. \qquad (9)$$

If the temperature is constant, the condition for no current is

$$eV+\zeta=\text{constant},$$

which is the usual condition that the total potential, electrical plus chemical, is constant in equilibrium. As is well known, the term $(\partial\zeta/\partial x)_T$ gives no contribution upon integration around the circuit. The rest of (9) is identical with (4).

[2] R. H. Fowler, *Statistical Mechanics* (Cambridge, 1936), second edition, p. 408.

Letters to the Editor

PROMPT publication of brief reports of important discoveries in physics may be secured by addressing them to this department. The closing date for this department is the third of the month. Because of the late closing date for the section no proof can be shown to authors. The Board of Editors does not hold itself responsible for the opinions expressed by the correspondents. Communications should not in general exceed 600 words in length.

The Origin of the $M\zeta_1$ and $M\zeta_2$ X-Ray Satellite Groups

FREDERICK R. HIRSH, JR.
University of Southern California, Pasadena, California
June 16, 1943

A PUBLICATION by Munier, Bearden, and Shaw[1] in September, 1940, revealed well-defined satellite groups for the x-ray lines $M\zeta_1$ and $M\zeta_2$. This very properly brings up the question of their origin. $M\zeta_1$ comes from the single electron transition $M_V \rightarrow N_{III}$, while $M\zeta_2$ arises from the transition $M_V \rightarrow N_{II}$. If, in accordance with previous work[2] on the Auger effect causing x-ray satellites, we ascribe the satellites just mentioned to initial MN ionization, we must choose a radiationless transition in the M-shells, which leaves the M_V shell and some N-shell ionized, and we see that $M_{III} \rightarrow M_V$ is the only possible radiationless transition:

$$(\text{Energy}_{M_{II}-M_V}) > (\text{any ionization energy for an } N\text{-shell})_{z+1}$$

for all atomic numbers (see Fig. 1); while

$$(\text{Energy}_{M_{IV}-M_V}) \ll (\text{any ionization energy for an } N\text{-shell})_{z+1}.$$

Hence there are no Auger "cross-overs" for the last-named bounding transitions, and the Auger effect cannot occur for them. Therefore, if the $M\zeta_1$ and $M\zeta_2$ satellites are due to the Auger effect producing MN ionization, the satellites may be accounted for by the following single electron transitions between doubly-ionized states:

$$\text{for } M\zeta_1, \quad M_V N_{IV,V} \rightarrow N_{III} N_{IV,V};$$
$$\text{for } M\zeta_2, \quad M_V N_{IV,V} \rightarrow N_{II} N_{IV,V}.$$

Then the satellites will be most prominent for atomic number 86, which is a few atomic numbers below $Z=88$, where the Auger "cross-over" occurs for $M_{III} \rightarrow M_V$ and the $N_{IV,V}$ shell energy curve (see Fig. 1).

It cannot be MO ionization which causes these satellites since:

For the O-shells (ionization energy)$_{z+1} \sim 2$ to 4 $(\nu/R)^{\frac{1}{2}}$ units; $(\nu/R)^{\frac{1}{2}}_{M_{III}-M_V} = 5$ to 6 $(\nu/R)^{\frac{1}{2}}$ units, too great an energy; $(\nu/R)^{\frac{1}{2}}_{M_{IV}-M_V} \sim \frac{1}{2}$ $(\nu/R)^{\frac{1}{2}}$ units, too small an energy for the Auger effect. Hence there will be poor wave function overlapping in these two limiting cases, and the Auger effect cannot exist, to cause MO ionization. For an illuminating plot of these data, see M. Siegbahn's *Spektroskopie der Roentgenstrahlen.*

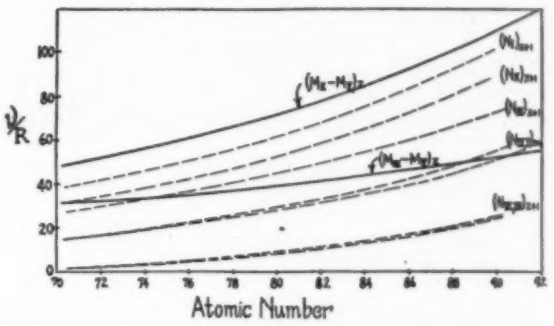

FIG. 1. Energy in ν/R units released by the radiationless transitions $M_{II} \rightarrow M_V$ and $M_{III} \rightarrow M_V$ (full lines), and ionization energies for the N-shells, plotted for $z+1$ as an M electron is missing (dashed lines).

[1] J. H. Munier, J. A. Bearden, and C. H. Shaw, Phys. Rev. **58**, 537 (1940).
[2] F. R. Hirsh, Jr., Phys. Rev. **50**, 191 (1936).

A Continuum in the 1849A Region in the Afterglow Spectrum of Mercury*

ALBERT WATTENBERG** AND HAROLD W. WEBB
Columbia University, New York, New York
June 10, 1943

MOORE and Garth[1] observed a continuous band in the afterglow spectrum of mercury vapor in the region 1849A which had not been previously reported. (Rayleigh[2] was unable to find either a line or a band in the afterglow in this region, even with extreme overexposure.) This same band was observed by Hamada[3] in a discharge in mercury in a Schuler tube, and was accounted for as being due to weakly bound quasi-molecules.[4]

We have further examined this diffuse band with one of the tubes employed by Moore and Garth, photographing with a small quartz spectrograph with Eastman II-O (U-V sensitized plates). A microphotometer record of this continuum is shown in Fig. 1. Trace A was made from a spectrogram taken with the spectrograph and the space between the slit and the quartz window of the discharge tube filled with nitrogen. Trace B was made from a spectrogram taken with air in the same optical path, and shows the O_2 absorption bands, which were useful in determining the wave-length scale. These spectra were made with a mercury vapor pressure of 0.8 mm. No appreciable change was observed in the distribution of the intensity

in the continuum with a fivefold change in the vapor pressure. The limits of this band are not definite, but most

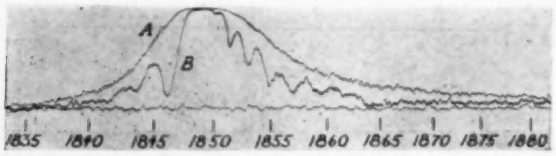

FIG. 1. Diffuse band in mercury afterglow. *A*—without oxygen absorption bands; *B*—with oxygen absorption bands.

of the energy is found between 1870A and 1835A with a maximum near 1849A.

* Publication assisted by the Ernest Kempton Adams Fund for Physical Research of Columbia University.
** Now at Metallurgical Laboratory, University of Chicago, Chicago, Illinois.
[1] R. Garth and G. Moore, Phys. Rev. **60**, 208 (1941); G. Moore and R. Garth, Phys. Rev. **60**, 216 (1941).
[2] Lord Rayleigh, Proc. Roy. Soc. **114**, 620 (1927).
[3] H. Hamada, Phil. Mag. **12**, 50 (1931).
[4] W. Finkelnburg, *Kontinuierliche Spektren* (Berlin, 1938), p. 202.

Erratum: The Mercury Arc Cathode

[Phys. Rev. 62, 48 (1942)]

C. G. SMITH
Raytheon Manufacturing Company, Newton, Massachusetts

THE Thomson heat was assumed to convect heat upward in the liquid mercury cathode, and the magnitude was calculated from an apparently erroneous formula taken from page 96 of the book, *The Metallic State* by Hume-Rorthery. The heat Q convected by unit current due to the Thomson heat σ acting in a region of thermal gradient $d\theta/dz$ was taken to be $Q=\sigma(d\theta/dz)$, as stated in the book. The convection of heat by unit electric current has been shown by Bridgman[1] to be $Q=\tau\int_0^\tau(\sigma/\tau)d\tau$. This is the heat convected past a point in a metal at absolute temperature T. Reasonable values of σ put into this formula lead to a value of Q only about 10^{-6} of that obtained by applying the first formula, under the assumed conditions.

Therefore, the simple assumption that Q was sufficient to counteract the thermal conduction $K(d\theta/dz)$ is not tenable without new considerations.

Recent observations of the continuous spectrum of the arc spot of the mercury arc cathode and observations upon a number of metallic arcs showing the peculiar retrograde motion in a transverse magnetic field, and other phenomena, are soon to be reported. In the report we expect to present a revised treatment of the thermal conduction problem in the cathode material as related to the Thomson heat.

The writer is very grateful to Dr. J. Slepian and to Mr. R. L. Longini of the Westinghouse Electric and Manufacturing Company for pointing out the error in the paper.

[1] P. W. Bridgman, *The Thermodynamics of Electrical Phenomena in Metals* (The Macmillan Company, New York, 1934), page 65.

Proceedings of the American Physical Society

STATE COLLEGE MEETING, JUNE 18 AND 19, 1943

THE 255th Meeting of the American Physical Society was held at State College, Pennsylvania, on Friday and Saturday, June 18 and 19, 1943. The American Association of Physics Teachers and the Pennsylvania Conference of Physics Teachers met with us, beginning their meetings on the previous Thursday evening. This was the second June meeting held in consecutive years at State College. Our hosts found themselves faced with much greater difficulties than those of the previous year, owing to causes which are too well known to require description. They acquitted themselves manfully in their double task, and the Society owes a great debt of gratitude to Dr. Wheeler P. Davey (Chairman of the Local Committee) and to many of his colleagues. One hundred and ten people registered from points other than State College; many of them did not have an easy journey.

The scientific programme included two symposia: "Physics in War Training Programmes" and "The Role of Physics in the Postwar Period." The former was designated as a symposium of the A.A.P.T., the latter as a joint symposium; actually, both were arranged by R. C. Gibbs. There were ten invited papers on our programme, most of them dealing with the use of physical methods in chemical analysis. Finally there were fifteen contributed papers, five of which (those numbered 5, 6, 7, 12, and 15) were read by title. The abstracts of the contributed papers and the titles of the invited ones are appended.

The dinner of the three Societies was held on Friday evening in the Nittany Lion Inn. Some of the officers spoke briefly, and the gathering was then addressed by W. R. Ham, of whom it should be said that he prepared his talk on twenty-four hours' notice in replacement of another speaker obliged to be absent.

At the Council meeting forty Members were elected; their names are appended. The Society had lost through death the following Fellows and Members: J. B. Engl (M), A. W. Goodspeed (F), J. Cramer Hudson (M), M. H. Kanner (M), C. M. Kilby (M), W. F. Magie (F). Mr. Magie was a former President of our Society. On June twenty-fourth occurred the death of another of our former Presidents and most distinguished Fellows, Joseph S. Ames.

The membership of the Society on June 17 numbered 4240.

Elected to Fellowship: Forrest F. Cleveland and Dean Woodridge.

Elected to Membership: Armistead, Fontaine C.; Barton, Charles A.; Bezuszka, Stanley J.; Billings, Bruce H.; Bittman, Loran R.; Burington, Richard Stevens; Butler, Howard W.; Chilton, Leonard Vincent; Cook, Emery Allen, Jr.; Day, Frank Hollingworth; Dodds, Wellesley; du Toit, S. J.; Falkoff, David L.; Frederick, Carl L.; Goldstein, Ladislas; Harris, Clyde W.; Krulikoski, Stanley, Jr.; Krumbein, A. Davis; Levine, Sol; Lewinstein, Max; Lockwood, Neil; Lund, Louis H.; Maduell, Charles Rene, Jr.; Monfore, Gervaise E.; Moon, Robert James; Moore, Carroll Lowry; Naiditch, Sam; Nierenberg, William A.; Peter, Brother Simon; Ramsey, Walter S.; Sausville, J. W.; Siegel, Edward; Simons, Charles Sands; Snyder, Frank D.; Stempin, Carl W.; Stimmel, Ronald G.; Terhune, Nelson A.; Van Poole, Thomas B., Jr.; Whitney Elliott; Zimmerman, John R., Jr.

SYMPOSIA

I. **Physics in War Training Programmes.**
II. **Role of Physics in the Postwar Period.**
R. C. GIBBS: **Some Problems Facing Physicists.**
G. P. HARNWELL: **Needs in Research.**
R. BOWLING BARNES: **Physics in Industry.**

INVITED PAPERS

W. F. G. SWANN: **Cosmic Rays.**
E. K. JAYCOX: **Modern Spectrochemical Analysis.**
NORMAN WRIGHT: **Physical Methods of Analysis and Control in the Chemical Industry.**
M. L. WILLARD: **Identification of Certain Organic Compounds.**
R. J. PFISTER: **An Addition to the Analytical Application of Raman Spectra.**

A. F. KIRKPATRICK: **Selective Dispersion: Physical Phenomena used in Quantitative Organic Analysis.**

C. E. WARING: **Magneto-Optic Rotation in Solutions.**

J. G. ASTON, G. J. SZASZ, H. L. FINK, and M. L. SAGENKAHN: **A Summary of the Work on Low Temperature Heat Capacities at the Pennsylvania State College during 1942–1943.**

J. E. NICHOLAS: **Some Preliminary Investigations on Dehydration of Fruits and Vegetables with Infra-Red Energy.**

KARL K. DARROW
American Physical Society
Columbia University
New York 27, New York

ABSTRACTS OF CONTRIBUTED PAPERS

1. The Viscosities of Pure Hydrocarbons and Lubricating Oils at Various Temperatures. M. R. CANNON AND J. M. GEIST, *Pennsylvania State College.*—Viscosity data were obtained for fifty-five hydrocarbons in the gasoline range at 0°C, 20°C, and 40°C. The measurements were made with modified Ostwald viscometers with water baths for temperature control. The viscosity-temperature behavior of the hydrocarbons followed the equation $\eta = Ae^{-B/RT}$. With this equation, the viscosities of the hydrocarbons may be calculated between 0°C and 40°C with a deviation of less than one percent. Some trends in the viscosity behavior of the measured hydrocarbons were noted. Among the octanes, the more compact molecules had the highest viscosities and viscosity-temperature coefficients. For the hydrocarbons which had approximately the same viscosities at 40°C, the alkylcyclopentanes had the lowest viscosity-temperature coefficients. They were followed by the alkylbenzenes, the alkylcyclohexanes, and the paraffins in that order. Vapor baths with automatic pressure regulation, which may be used for temperature control between 100°F and 500°F, were constructed. However liquid baths were preferred up to 210°F. The viscosities of three lubricating oils were determined at 100°F and 210°F using water baths, and at 300°F, 400°F, 450°F, and 500°F using the vapor baths. Their viscosity-temperature behavior did not follow the above equation. The measured viscosities of the lubricating oils were compared with values read from A. S. T. M. Viscosity-Temperature Charts. Above 300°F the chart values were always higher than the measured viscosities, by as much as ten percent at 500°F.

2. Solvent Extraction. K. A. VARTERESSIAN, *Pennsylvania State College.*—Solvent extraction is steadily taking its place as a unit operation in chemical engineering. Like most of them, it is primarily physical in nature. In an endeavor to understand its theory and practice, solvent extraction may be divided into the following: (a) equilibrium relationships (b) methods of operation (c) design of equipment and (d) applications in various industries. The art and science of extraction has profited a great deal by analogy with the more widely used and discussed unit operation of distillation; thus the concepts of similarity between heat and solvent and between vapor pressure and osmotic pressure have aided in organizing the subject matter, especially with regard to solvent economies, equilibrium relationships and efficiency factors. On the other hand, analogy with the unit operation of absorption has been of assistance in formulating rate and capacity equations and a view of extraction mechanism. Extraction with solvent is an effective tool in the separation of complex solutions into their component parts. It is particularly adapted to the segregation of substances having high boiling points and susceptible to decomposition. The analysis of residual petroleum oils by means of extraction with acetone at room temperature is an illustration of the numerous potentialities of this unit operation.

3. An X-Ray Study of Brasses Formed by the Interdiffusion of Copper and Zinc Deposited on Glass by Evaporization. ARTHUR A. BURR, H. S. COLEMAN, H. L. YEAGLEY, AND W. P. DAVEY, *Pennsylvania State College.*—By using the technique developed by Coleman and Yeagley, alloys were made by the interdiffusion of films of copper and zinc deposited on glass microscope slides by vaporization methods and x-ray investigations carried out. Data were obtained by means of the standard photographic powder method and by means of the Penn State Automatic X-Ray Spectrometer. Metal films used were of the order of 6×10^{-5} cm in thickness. (1) It is shown that the metal films formed on glass by vaporization and the resulting alloys formed by diffusion have the same crystal structure as the bulk metal. (2) A series of samples in the beta brass range were subjected to heat treatment at 198°C for varying lengths of time. Their diffraction patterns show that formation of any higher phase by diffusion involves temporary existence of all the other copper-zinc phases as intermediate stages. (3) Diffraction patterns recorded by the Automatic Spectrometer show orientation in the films. This gives experimental support to a proposed picture of the nature of phase changes during diffusion based on calculations from the lattice parameters. Techniques and procedure developed in this work suggest a method of determination of constitution diagrams and diffusion rates at low temperatures.

4. Tables of Intensity Ratios for Scattered Molecular Beams. JOHN K. WOOD, *Pennsylvania State College.*—In the interpretation of data of experiments on the scattering

of molecular beams by molecular clouds, graphs of a non-integrable function are required. The beam intensity ratio before and after scattering is a function of the temperatures of the beam molecules and of the temperature of the scattering cloud of molecules thus giving a family of curves of intensity ratios against one temperature function, the other being a variable parameter. The integral contains a term determined by a wave mechanical consideration of the problem of collisions and does not yield a simple closed solution because of this factor. The trapezoid rule for numerical integration was used in preference to Simpson's rule since it gave a smaller error to the numerically summed integral when the molecular cloud temperature was zero. The theoretical value of the integral at this point of no scattering is 1.000. Errors were taken at this point because on integrating again with a smaller interval of the dependent variable the first point showed the largest deviation from the more accurate integration. The tables have a temperature range which will cover most experiments using Li, Na and K.

5. Further Facts Concerning the Magnetic Current. FELIX EHRENHAFT, *New York City.*—The hypothesis of the electric current was founded chiefly upon three facts: The existence of electric ions, the decomposition of water (electrolysis), the circulation of the single magnetic pole around the constant electric current. Now those three facts have been observed in magnetism as well: the existence of magnetic ions, the decomposition of water through the magnet (magnetolysis), the circulation of a single electrostatic charge around the constant magnetic current. In the microscope one observes that different gas bubbles as well as solid particles move in circles around the axis of the magnet simultaneously in opposite directions. Each of them reverses its direction of motion with the reversal of the magnetic field. The bodies carry positive or negative electrostatic charges. The existing laws of electrodynamics (Biot-Savart, H. A. Lorentz) cannot explain the new facts because the electrostatic charges in question are resting ones, etc. Just as the line integral of the magnetic force defines the intensity of the electric current (Ch. Oersted, A. M. Ampere), the line integral of the electric force defines the intensity of the magnetic current. Electricity and magnetism represent an indivisible union, reaching far above the union established by Faraday, Maxwell, and Hertz. The electrodynamic equations must be extended to include the term of the magnetic current. These theses will be illustrated by microphotographs of the experiments.*

* The experiments can be seen at C. Zeiss Inc., New York City.

6. Use of a Mass Spectroscope in Artificial Radioactive Assignments. W. M. SCHWARZ AND M. L. POOL, *Ohio State University.*—At a number of places throughout the array of stable and artificial radioactive isotopic positions unequivocal assignments of activities to definite mass numbers are very difficult or impossible even with the aid of various bombarding particles and exacting chemistry. Consequently a modified Nier type mass spectrograph was adapted for use with artificial radioactive sources. The source of ions was a high frequency spark between solid electrodes which previously had been made radioactive. Very strong and highly concentrated activities are needed for satisfactory operation. The method was checked with the 12-hour radioactive copper period. Zirconium bombarded with deuterons yielded two periods of 23 hours and 18 days which have in addition to previously reported characteristics gamma-rays energies of 1.1 and 0.97 Mev, respectively.

7. Radioactivities in Barium Obtained from Cesium. KATHERINE E. WEIMER, M. L. POOL, AND J. D. KURBATOV, *Ohio State University.*—Additional observations on the artificial radioactivies induced in barium indicate that a very long period of several months is obtained by the Cs+*d* reaction in addition to the previously reported period of 38.8 hours. The long period emits x-rays characteristic to the cesium region as well as gamma-rays. Repeated purifications identify this long period chemically as barium. After several months following a bombardment chemical separations of the barium fraction from bombarded cesium yielded no activity. Therefore this period seems best assigned to Ba^{133}. The previously reported 14.2-day period obtained from Cs+*d* was not observed from Hilger spectroscopically pure cesium. Proton bombardment of cesium yielded a single period of 38.8 hours also assigned to Ba^{133}.

8. Determination of Nuclear Moment of Rubidium by Resonance Radiation. RALPH ATHERTON, *Miami University.* (*Introduced by R. L. Edwards.*)—Radiation of λλ4201.8A and 4215.56A from a hydrogen-rubidium discharge tube was focused on a resonance chamber containing distilled rubidium. Resonance radiation from this chamber was photographed through Wollaston and Nicol prisms. The percentage of polarization was calculated from these plates and the results compared to theoretical calculations based upon nuclear moment assignments for rubidium made by Jackson. The agreement seemed to be well within experimental error.

9. Sensitized Fluorescence and Tesla Discharge Spectra of Chromium Vapor. J. G. WINANS AND W. J. PEARCE, *University of Wisconsin.*—The Tesla discharge and sensitized fluorescence spectra of chromium vapor have been obtained with the simplified procedure that was followed for lead and indium.[1] Electrolytic metallic chromium was crushed to a powder and inserted in the quartz tubes before evacuation. The completed tubes contained only mercury and powdered chromium. Spectra were obtained with different mercury pressures from about 0.1 to 15 cm. The temperature was kept as high as possible without collapsing the quartz tube. About fifty chromium lines have been

identified in the Tesla discharge spectra at medium to high mercury pressures. Six lines (the two resonance triplets at 3600 and 4300) have been obtained in sensitized fluorescence. No action of selection rules for excitation of Cr by collision of the second kind is indicated by results so far obtained.

[1] J. G. Winans, Francis Davis, and Victor Leitzke. Pb Abstract, Phys. Rev. **55**, 1126 (1939). In Abstract, Phys. Rev. **57**, 70 (1940).

10. Exterior Ballistics of Small Arms Ammunition. RALPH HOYT BACON, *Frankford Arsenal, Philadelphia, Pennsylvania.*—Previous measurements of the time of flight and of the velocity of small arms bullets have involved firing through two or more screens of some kind. These screens, of course, affect the flight of the bullet, so that it was seldom feasible to fire through more than three screens at once. Furthermore, in order to obtain velocities and times of flight as functions of the distance, it was necessary to fire a few bullets through a set of screens placed at some chosen distances, and then to fire another group of bullets through another set of screens at another set of distances, and then try to make the sets of results agree. The equations thus obtained are generally quite complicated. However, a bullet in flight carries a small electrostatic charge. The arsenal has developed apparatus for detecting the passage of these charged bullets through the plane of a loop of thin wire, without interfering with the flight of the bullet. By firing bullets through a series of such loops, and recording the transit of the bullets on a suitable chronograph, the following remarkably simple equation was obtained for velocities between 2000 and 3000 feet per second: $dv/dt = -kv^{3/2}$.

11. Isobary—A Criterion for the Stability of the Lithosphere. ROSS GUNN, *U. S. Naval Research Laboratory, Washington, D. C.*—A quantitative investigation is made of the influence of a strong elastic lithosphere on departures from isostasy. Isostasy is shown to be a special case of a more general principle that may be called the principle of isobaric equilibrium. This principle which expresses the condition for vertical equilibrium is formulated quantitatively both in terms of the resultant vertical stresses in the lithosphere and in terms of measurable gravity anomalies. Employing the principle, a stress function may be determined that permits an estimate of the fraction of the uniform superposed load actually carried by the lithosphere. By applying this method, it is found that even for the central region of a block load to be in substantial isostatic adjustment (96 percent), the linear dimension of the load must approximate 330 km, a value more than six times that often assumed. The deformed figures of the lithosphere for certain special types of load have been worked out together with the stress function that measures both the gravity anomaly and the resultant vertical stress. The resulting distributions of displaced mass that compensate for various types of earth features are found to be not at all like the distributions usually assumed in isostatic reductions.

12. Heat Conduction in Blocks and Cylinders. C. B. POST, *The Carpenter Steel Company, Reading, Pennsylvania.*—Solutions of the heat-conduction equation are discussed for computing the rates of cooling at 1300°F during quenching in various finite sections such as cylinders, bars and blocks. The proposed method utilizes simple combinations of the temperature functions for the quenching of cylinders of infinite length and slabs for which tables are available. These calculated rates of cooling in finite sections are used to determine hardness contours in hardened steel blocks and cylinders. Data are presented showing the comparison of calculated and experimental hardness contours in various steel shapes.

13. Supersonic Measurements in Gases. W. H. PIELEMEIER, *Pennsylvania State College.*—A number of previous investigations of the velocity and the absorption of sound waves in gases were reviewed. Curves are shown for V_0, the velocity of low frequency and of V_∞, the velocity of high frequency sound waves in dry CO_2 as a function of temperature from 0 to 100°C. Another set of curves shows how f_m, the frequency producing maximum absorption per wavelength depends on the water vapor concentration in the CO_2 at approximately one atmosphere pressure. Evidence is presented for *two* distinct relaxation times for each given concentration. Most of this evidence is found in the published work of Knudsen and his students and in our data. A number of investigators have doubted the existence of two distinct relaxation times in CO_2. Acetaldehyde[1] has recently been investigated and was found to have three distinct relaxation times. Our measurements with helium of high purity show that the specific heat agrees well with the theoretical value and that the absorption agrees better than earlier results. Byers' work in this laboratory with carbon tetrafluoride furnishes a reliable value for the specific heat and for the relaxation time of CF_4.

[1] Alexander and Lambert, Proc. Roy. Soc. **179**, 499 (1942).

14. Measuring Small Increments of Length by Hydraulic Michelson Interferometer. C. G. STERGIOPOULOS, F. H. NADIG, AND J. L. BOHN, *Temple University.*—By applying hydraulic magnification to move one of the mirrors of the Michelson interferometer, increments of length of the order of 10^{-7} cm are detected. The apparatus consists essentially of two vertical cylinders of different diameters, partially filled with mercury and connected at the lower ends. Each is fitted with a freely moving plunger. Displacement of the large plunger is detected by the interferometer, one of whose mirrors is fixed to the smaller plunger. To verify the magnification as given by the dimensions of the apparatus, readings on this apparatus were compared with readings on a conventional Michelson interferometer. The instrument was used in the measurement of magnetostriction but can be applied to other small changes in length or may be used as a surface roughness indicator.

15. The Application of Multiplier Photo-Tubes to Quantitative Spectrochemical Analysis. E. A. BOETTNER, *Wyandotte Chemicals Corporation, Wyandotte, Michigan,* AND G. P. BREWINGTON, *Lawrence Institute of Technology, Detroit, Michigan.*—A bridge circuit consisting of two multiplier photo-tubes (RCA 931) has been adapted to indicate the ratio of intensities of spectral lines when the tubes are mounted on a spectrograph in place of the photographic film. It has been found that holding the voltage constant on one tube (set on an internal standard line) and varying the voltage applied to the other tube (set on an impurity line), the plot of the logarithm of the concentration of the impurity in the source *vs* the difference of voltage applied to the two tubes is a straight line. Quantitative analyses made using this circuit and calibration method have approached and in some cases equaled the accuracy and sensitivity possible with a photographic plate. Some indication has been obtained that if proper light sources were available the galvanometer reading representing unbalance of the bridge might be of significance for quantitative analyses.

AUTHOR INDEX TO ABSTRACTS OF THE STATE COLLEGE MEETING

Atherton, Ralph—No. 8

Bacon, Ralph Hoyt—No. 10
Boettner, E. A. and G. P. Brewington—No. 15
Bohn, J. L.—see Stergiopoulos, C. G.
Brewington, G. P.—see Boettner, E. A.
Burr, Arthur A., H. S. Coleman, H. L. Yeagley, and W. P. Davey—No. 3

Cannon, M. R. and J. M. Geist—No. 1
Coleman, H. S.—see Burr, Arthur A.

Davey, W. P.—see Burr, Arthur A.

Ehrenhaft, Felix—No. 5

Geist, J. M.—see Cannon, M. R.
Gunn, Ross—No. 11

Kurbatov, J. D.—see Weimer, Katherine E.

Nadig, F. H.—see Stergiopoulos, C. G.

Pearce, W. J.—see Winans, J. G.
Pielemeier, W. H.—No. 13
Pool, M. L.—see Schwarz, W. M.
—— see Weimer, Katherine E.
Post, C. B.—No. 12

Schwarz, W. M. and M. L. Pool—No. 6
Stergiopoulos, C. G., F. H. Nadig, and J. L. Bohn—No. 14

Varteressian, K. A.—No. 2

Weimer, Katherine E., M. L. Pool, and J. D. Kurbatov—No. 7

Winans, J. G. and W. J. Pearce—No. 9
Wood, John K.—No. 4

Yeagley, H. L.—see Burr, Arthur A.